Study of the modeling of rice cultivation under different irrigation systems and planning in the district of UsoCoello and analysis of the model applied to the region of Tolima in Colombia

Auteur : Chavet, Maxime
Promoteur(s) : Wellens, Joost
Faculté : Gembloux Agro-Bio Tech (GxABT)
Diplôme : Master en bioingénieur : sciences et technologies de l'environnement, à finalité spécialisée
Année académique : 2021-2022
URI/URL : http://hdl.handle.net/2268.2/16006

LIÈGE université
Gembloux
Agro-Bio Tech

Master Thesis Report

Study of the modeling of rice cultivation under different irrigation systems and planning in the district of UsoCoello and analysis of the model applied to the region of Tolima in Colombia

Maxime Chavet

END OF STUDY WORK SUBMITTED IN VIEW OF OBTAINING THE DIPLOMA OF MASTER BIOENGINEER IN SCIENCES AND TECHNOLOGIES OF THE ENVIRONMENT

ACADEMIC YEAR 2021-2022

PROMOTOR: Pr. Joost Wellens

CO-PROMOTOR: Pr. Sofiane Ouazaa

LIÈGE université
Gembloux
Agro-Bio Tech

Master Thesis Report

Study of the modeling of rice cultivation under different irrigation systems and planning in the district of UsoCoello and analysis of the model applied to the region of Tolima in Colombia

MAXIME CHAVET

END OF STUDY WORK SUBMITTED IN VIEW OF OBTAINING THE DIPLOMA OF MASTER BIOENGINEER IN SCIENCES AND TECHNOLOGIES OF THE ENVIRONMENT

ACADEMIC YEAR 2021-2022

PROMOTOR: Pr. Joost Wellens

CO-PROMOTOR: Pr. Sofiane Ouazaa

Acknowledgements

Dans le cadre de la rédaction de ce TFE, je souhaite tout d'abord remercier le personnel enseignant de l'université de Gembloux, notamment Sarah Garré et Joost Wellens, et le groupe de recherche RiceClimaRemote, notamment Sofiane Ouazaa et Ronald Martinez, pour leur encadrement, pédagogie, connaissances et idées novatrices pour le futur, m'ayant permis d'avoir l'opportunité de m'enrichir sur beaucoup de plans, autant scientifiquement, que socialement et culturellement au travers de ce travail.
Je ne serai jamais assez reconnaissant vis-à-vis de ma famille, mes parents, ma soeur, qui ont été toujours été là pour moi, pour me soutenir, m'encadrer, me fournir une éducation et faire en sorte que je ne manque de rien. Mais aussi pour mes amis, dont certains présents depuis l'enfance ont fait le nécessaire pour ne jamais perdre les liens, mais aussi les formidables personnes recontrées à Gembloux, ambitieuses de projets et remplies d'idées, qui ont pu m'inspirer et aux côtés desquelles j'ai pu cultiver différents projets et passions, mais aussi des moments délirants, mémorables et toujours pleins d'aventure.

Abstract

The management of irrigation districts is becoming laborious in some regions of Colombia. In the Tolima region, the bimodal climate is present in hot and semi-arid areas that are vulnerable due to the increasing impact of climatic phenomena that cause an intensification of droughts, but also of rainfall. The systems in place sometimes require more water than is needed, in a context of increasing producer density. Agricultural yields, particularly for rice, which is very present in the region, can sometimes decrease in an unprecedented way in the event of insufficient water supply. Moreover, the experiments to be carried out to put an end to these problems are sometimes costly in terms of time and money. In this study, trials of irrigation systems and scheduling were tried, and the use of a calibrated crop simulation model to assess the possibility of predicting the behaviour of these experiments on a variety of *Oriza sativa* L. from the region. The calibration shows simulations of the evolution of plant parameters, such as canopy cover with an average RMSE of about 2.60% and correlated for the first cycle and a much poorer simulation for the second cycle, but also a simulated dry yield with an overall MBE of 0.621t/ha that is rather accurate and can differ from the observed evolution of the different treatments to some extent. Further simulations were carried out to assess the importance of the parameters on these outputs. The sensitivity analysis shows 7 parameters explaining 95% of the total sensitivity of the evolution during a fictitious cycle of different soil water content, biomass, canopy cover and dry yield. These results will allow future evaluation of irrigation schedules in order to optimise yields according to local water consumption. Based on the results of the sensitivity analysis, further analyses can be done in the region to facilitate and plan future calibrations in a local environment. Thanks to the processed and modelled local climate data, it will

also be possible to carry out irrigation schedules according to extreme weather events.

Table des matières

Contents

1 Abbrevations

- AWC: Available Water Content
- AWD: Alternate Wetting and Drying
- C1: Cycle 1
- C2: Cycle 2
- CC: Canopy Cover
- CN: Curve Number
- CSM: Crop Simulation Model
- DAS: Days After Sowing
- ENSO: El Niño-Southern Oscillation
- FAO: Food and Agriculture Organization of the United Nations
- F67: Fedearroz 67 variety
- GDD: Growing Degree Day
- HI: Harvest Index
- IDEAM: El Instituto de Hidrología, Meteorología y Estudios Ambientales
- MBE: Mean Bias Error
- MIRI: Multiple Inlet Irrigation system
- MPE: Mean Percentage Error
- PWP: Permanent Wilting Point
- RMSE: Root Mean Square Error
- TAW: Total Available Water
- UAV: Unmanned Aerial Vehicle

2 Introduction

Only 2.8 % of the water on Earth is fresh. Less than 0,02% of the earth's water is both fresh and liquid, and therefore useful for consumption or agriculture. 70% of the world's freshwater is used for agriculture and rises to 90% in some developing countries. Some of the freshwater in aquifers (30%) is also non-renewable. Some aquifers, sometimes with non-renewable water, are accessible and are exploited for domestic, agricultural or industrial uses, while other aquifers are inaccessible (Gleick & al., 2010). More and more water conduits are being dug. Among the 37 largest aquifers in the world, 21 are being exploited unsustainably: they are being drained by humans faster than nature can recharge them (Richey & al., 2015). The demands placed on land and water resources are greater than they have ever been, and their accumulation is pushing the productive capacity of water and land systems to the limit. Between 2000 and 2019, irrigated crops doubled while rainfed crop growth grew by only 2.6% during the same period and the amount of agricultural land per person that could be used for crops and animal husbandry decreased by 22% due to population growth but also because of trends toward more water-intense lifestyles and diets. Approximately 300 million ha of land are already irrigated globally, and although water is a renewable resource, some projections indicate a developing water consumption for agriculture. Providing food and fiber for almost 8 billion people worldwide in the face of depleting freshwater supplies is agriculture's biggest issue (FAO, 2021).

Among these irrigated crops, rice (*Oryza sativa* L.) is the most important cereal crop in the developing world and is the staple food for more than half the world's population (FAO, 2001). Rice irrigation has mainly bassin and border surface irrigation systems (Sauer & al., 2010; Fischer & al., 2012) and, in general, surface irrigation is the most dominant system in Colombia (Siebert & al., 2015). Surface irrigation systems have lower application efficiencies, thus more non-beneficial water consumption, than others systems due to runoff and deep infiltration losses, mainly for bassin and border systems (Sauer & al., 2010; Jägermeyr & al., 2015; US EPA, 2017). Colombia has rice crops supplied either in water by rain, either by irrigation. In some parts of Colombia, especially in the north and in the central massif, there are regions with semi-arid and arid climates. Something that could be a problem is that some central Colombia areas, such as the region of Tolima, require investments that are expensive in terms of irrigation systems but allow for the production of rice twice a year due to the bimodal climatic behaviour that varies between dry and rainy periods (Redagricola, 2021), and more precisely a warm semi-arid climate according to the Caldas-Lang classification with an average annual temperature between 27 and 30°C and an average annual precipitation between 1300 and 1900 mm making it one of the driest regions in the country (IDEAM, 2014). Moreover, Tolima is the second largest department with the largest rice production area in Colombia (Redagricola, 2021) among the 18 others (Minagricultura, 2018) and provide the value of this highest crop yield per hectare in 2020 and 2021 (DANE, 2021). An analysis performed on QGIS 3.24 with the Land Use Land Cover CORINE classification data from IDEAM (2018) shows that rice cultivation in Tolima accounts for 77% of the area allocated to permanent or transitional agriculture and 99,5% of the transitional crop. Transitional crops such as rice require 35% of the total annual demand and 21% of extracted water is not consumed in 2014 (IDEAM, 2014).

Crops in the Tolima valley are irrigated by several irrigation districts. The UsoCoello district is one of these and will be the focus of this study. It is fed by the Coello river from the west and the Hormiga river from the east. Within this district, rice cultivation represents 98% of the surface area, beside oil palm and other permanent tree crops. Data from IDEAM (2014) show an annual water consumption of over $200m^3$/year for the area fed by the Coello, Cucuana and Hormiga rivers, one of highest levels in the country. The central-eastern Tolima region is among the regions in the world where the ratio of freshwater taken by the agricultural, industrial and municipal sectors to the total amount of renewable freshwater is between 75 and 100 percent in 2018, indicating sometimes very high water stress (FAO, 2021). Moreover, excessive irrigation water and poor drainage may lead to

groundwater pollution, especially through the use of agrochemicals, and soil salinisation, which may affect soil structure or make water difficult to access for plants (Shah & al., 2000).

Coupled with this high consumption of water which is not always used by the plant, global warming due to human activities, and associated with the "El Niño" climate phenomenon, could further limit water availability to crops in the coming years due to droughts. This could impact on water availability if not optimally used, and thus reduce crop yields. The consequences of the climate phenomena "La Niña" and "El Niño" are respectively the result of the cooling and warming of the Pacific Ocean on the west coast of the South Ameri continent. The amplitude of the "El Niño-Southern Oscillation" (ENSO) and the frequency and duration of large-scale events have been higher since 1950 than since 1850-1950 (Christensen et al., 2013). "El Niño" events occur irregularly, every 2 to 7 years. In the Tolima region, "La Niña" causes more frequent decreases in temperature and increases in precipitation, whereas it's the opposite is for "El Niño" (Peña & al., 2014). During the "El Niño" events of 2015, 2016 and 2019 (NWS NOAA, 2022), a reduction of at least 10% in rice yields compared to the previous year is observed in the Tolima region (DANE, 2021). In such drought cases, a rotation system is adopted in the UsoCoello district, dividing the 200 plots present into three groups, two of which will have access to water for six days and one for three days. At the end of these three days, the roles are exchanged and the farmer can again have access to water for 6 days, while another loses it for 3 days. This may represent a risk of water stress for the crops in the group without access to water if severe droughts occur and the water supply becomes limited.

Access to Tolima's irrigation districts has increased land prices, which have been widely subdivided, implying a much greater growth of producers than in the rest of Colombia since 1980. In Colombia, much of the agricultural land is owned by landlords who rent it to farmers on a temporary period. In the first semester in 2016 in Tolima, the areas sown in irrigated rice by tenants were 56 % and in rainfed rice 75 %. It implies that in the rice sector, rice production is in the hands of tenants, which is not the best thing in the long term, as the investments made are generally short term and investments are not necessarily made in technology to improve productivity and even less in intra-farm infrastructure. Because of this, agricultural practices that would allow for more sustainable land use are rarely considered (FEDEARROZ, 2021). In the UsoCoello district, land is devoted to monoculture and sometimes left to graze. In these soils, the structure is sometimes severely altered as a result of constant ploughing or disking to the same depth, allowing the passage of heavy agricultural machinery, especially on wet soils, the using of a limited crop rotation without variability in root structure or rooting depth, and the using of heavy equipment for construction site preparation or land levelling (Raes & al., 2018). This may lead to compaction and the formation of a hardpan that may affect the plant development. Micropores grew at the expense of macropores during compaction (Ghildyal & Satyanarayana, 1965), decreasing the total available water for plants. Globally, 49% of agricultural land was considered degraded or deteriorated by humans in 2015. South America is the second region in the world with the highest amount of land degraded by humans (FAO, 2021). In conclusion, there is a growing number of users to satisfy in a context of soil degradation and water loss due to excessive non-optimised consumption in crops that can affect the environments conducive to production in the long term, but also to climatic phenomena that are intensifying and making water resources scarce.

The goal is thus reducing water consumption on rice crops and increasing the ratio of water only useful to the root zone to water applied. Other more economical irrigation techniques applicable to rice cultivation have already been tested , such as furrow irrigation or sprinkler irrigation. However, yield reductions on rice with sprinkler irrigation have already been observed in the USA (McCauley, 1990; Wescott & Vines., 1986), as well as with furrow irrigation (Vories & al., 2002). Among these systems, Multiple Inlet Irrigation (MIRI) allows for a better distribution of irrigation by flowing water through a pipe along the length of the plot, which will exit through hatches separated by equal distances. The water flows simultaneously over the plot between and over bunds located parallel to

each side of the holes in order to distribute more uniform amounts of water. Vories & al. (2005) have practised this technique in Arkansas and have observed equivalent or higher rice yields with the MIRI system compared to the conventional board irrigation system. Water savings with MIRI ranging from 23 to 24 % have been observed among 19 counties on different soil types (Tacker & al., 2002). Trials carried out in the Tolima region have demonstrated a reduction in the volume of water applied of 35 % (FEDEARROZ, 2017). Between 2017 and 2019, there has been a 5 % growth in the total rice cultivation area of Tolima under MIRI and Tolima is the region with the most cultivation under MIRI in Colombia in 2019 (FEDEARROZ, 2020). An interesting and easy-to-use type of irrigation scheduling is the "Alternate Wetting and Drying" (AWD). These are perforated tubes driven into the soil to measure the height of water in the soil. The irrigation cycles involve flooding the soil, letting it dry to a specific depth below the soil surface, then rehydrating it to begin the cycle again (Price al., 2013; Carrijo al., 2017). There are different recommended depths that will vary the length of the cycle to be calibrated depending on the soil and environment (Price al., 2013; Lampayan al., 2015). AWD method uses up to 35 % less water and, mostly depending on the soil conditions, can result in yield maintenance, yield gains of 10 %, or modest production decreases (Price al., 2013). AWD is also an increasingly common system in Colombia and Tolima and provides better water savings (SATREPS, 2019). Other systems exist such as the Groud Cover Production System, or the intensive rice system using less water than a conventional border irrigation system, but MIRI and AWD may consume less water than the latter and MIRI offers the highest yield in the tropics (Gonzalez Alonso, 2016). Three plots with one treatment each were tested at the AGROSAVIA research centre at Nataima in the UsoCoello district. One plot with a MIRI system with AWD, one MIRI plot without AWD and one control plot with border irrigation.

To address these issues, various measures can be explored. Irrigation calendars based on ENSO events should be created for rice irrigations with recent years data in the UsoCoello district. Moreover, the impact on yields of using new, more water-efficient and more optimally planned irrigation systems therefore requires further study. To help to that, crop simulation models (CSM) are a more time and cost efficient way to assess crop yield response to irrigation under various field conditions than field experiments (Boote & al., 1996; Rosenzweig & al., 2014). Crop simulation models (CSMs) are particularly used in arid environments to evaluate the evolution of crop biomass as a function of management practices or irrigation schedules. Several models, including WOFOST (Diepen Van, 1989), DSSAT (Jones & al., 2003) and CropSyst (Stöckle & al., 2003), have been validated and compared (Touré & al., 1995; Todorovic & al, 2009) with the aim of better understanding crop response to climate and management scenarios, knowing that each model has its own strengths and weaknesses (Fraisse & al., 2006; Resop & al., 2012). For this reason, the Food and Agriculture Organization of the United Nations (FAO) developed the Aquacrop model in 2009 to balance simplicity, robustness and accuracy based on a water management approach (Raes & al., 2009; Stedulo & al., 2009; Hsiao & al., 2009; Vanuytrecht & al., 2014). The latter is more appropriate for farmers than the more complex models available (Abedinpour & al.,2012), takes into account crop water stresses (Geerts & al., 2010; Abedinpour & al.,2012), has been validated for different crops and widely used to develop irrigation schemes to ensure yield production (Geerts & al, 2010; de la Casa & al., 2013; Zhai & al., 2019), allows quantification of water used (Gobin & al., 2017; Kersebaum & al., 2016), is useful for assessing climate changes on crop yields (Vanuytrecht & al., 2014; Garofalo & al., 2019) and for developing support and decision tools for producers (Cusicanqui & al., 2013). The idea of this work is to calibrate a crop model, in this case Aquacrop, in order to evaluate how well it can predict crop yields as a function of the treatment applied, but also the evolution of the crop over time and the behaviour of water in the soil.

Simulation of rice cultivation under AWD with Aquacrop has already been carried out in Peru evaluating different water depths, showing good modelling of the evolution of canopy cover, grain yield and soil water content (Porras-Jorge & al., 2020), but also in the Middle East, showing good modelling

of crop yields (Ebrahim & al., 2015; Mirfenderski & al., 2022). In contrast, no studies were found on crop evaluation under MIRI with Aquacrop. Aquacrop allows the calibration of crop parameters, some of which are conversative and should not be changed, while others are calibratable because of their variability depending on the environment, crop management or genetic selections and varieties created accross the years (Raes & al., 2018). A calibration of a rice variety originating from the Philippines under transplantation crop was calibrated in Peru with three treatments maintenances of different levels of tension in the soil (Melo Solarte, 2019). No work was found on the calibration of Aquacrop in Colombia for local rice varieties under MIRI or MIRI combined with AWD irrigation scenarios. This work will focus on the calibration of the variety Fedearroz 67 in the Tolima region and more specifically in the UsoCoello district based on two crop cycles measurements. This will allow an assessment of how well the model simulates the observed yields and with the same order of growth between the three treatments.

Despite being simple as possible to use and transparent, AquaCrop nevertheless includes 43 parameters that must be calibrated (Vanuytrecht & al., 2014). The optimal collection of experimental data comes from contrasting experimental settings that match with model output variables such as biomass, canopy cover, dry yield, soil water content,... (He & al., 2017). The strategies of the experimental design can be of different nature : (1) Capturing variation in the data by measuring more output variables or increasing the frequency of observations (e.g., from monthly to weekly), (2) Introducing more variation in the data through multiple locations/multiple years of field experiments with various treatments (such as irrigation, fertilization levels, etc.) (Coudron & al., 2021). But sometimes, in reality, these measurements require a lot of financial ressources and is time-consuming. The crop calibration can also be done on the basis of literature data, or on the basis of aerial or satellite remote sensing data to define crop canopy cover (Mauria & al., 2018; Durfee & al., 2019), and phenological stages (Wang & al., 2014). However, costly in-situ measurements are still required. As a result, careful consideration should be given to the experimental design and data needs for model parameter estimation. This could be made through a sensitivity analysis. To launch this with a correct set of parameters, the model's output variables must be sufficiently responsive to changes in each individual parameter, and changes in the other parameters may not entirely make up for changes in the model outputs brought on by a change in a single parameter (Omlin & al., 2001; De Pauw & al., 2008). This would allow to know which experiment steps have to be prioritised to improve the precision of some outputs. Local sensitivity analysis is used to generate sensitivity functions, however it has limitations in terms of resilience over a wider parameter range (Saltelli & Annoni, 2010). Therefore, global sensitivity techniques are maily used over local sensitivity analysis, such as the Morris method (Morris, 1991) or E-FAST (Saltelli & al., 1999). A study has already been carried out on the variability of 34 input parameters with local plausible values on six output variables of Aquacrop, of soil water content and of crop simulations, about potato cultivation in Belgium taking into account environmental (soil and climate) and annual variability, the results made it possible to evaluate the importance of each input parameter on the results under these conditions (Coudron & al., 2021). The present work will be the subject of a similar study on rice cultivation in the Tolima region.

3 Material & Methods

3.1 Experimental device and irrigation management

An experiment was carried out on two rice cropping cycles of three plots, each comprising four SPLIT-PLOT replicates, considering two factors: three different combinations of irrigation methods and schedules and two 124-day cropping cycles before the harvest. The first crop cycle took place between the May 12 and the September 15 2021 and the second crop cycle between the December 4 2021 and the April 6 2022. The layout of the two cycles and the plots is shown on the fig. 1.

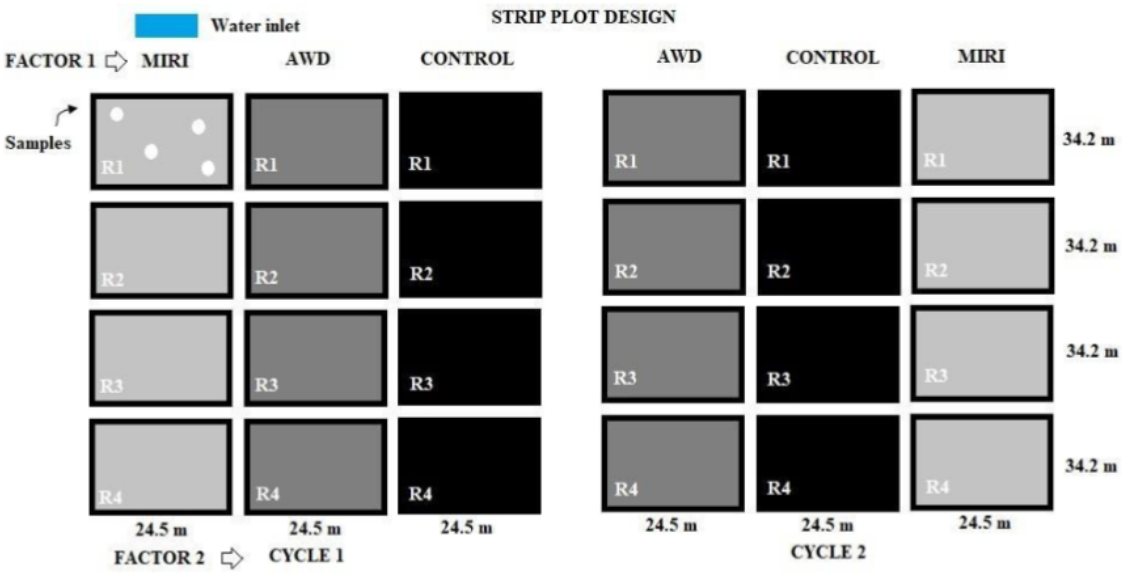

Figure 1: Scheme of the plots layout from RiceClimaRemote (2021)

Figure 2: Experimental plots of rice cultivation

According to the level at which the soil is permitted to dry, there are three types of AWD: "mild or safe," where the water level stays over 15 cm below the soil; "moderate," where it stays above 25 cm; and "severe," where it stays above 30 cm (Lampayan & al., 2015). When first it's the first use, safe AWD is advised; after that, the depth can be raised (Norton & al., 2017). For the AWD method, the irrigation scheduling was performed using the indicator tubes,re-watering after the tube water lowers 15cm below the soil surface (mild AWD). Watering saturates the soil to about 5cm. The irrigation scheduling for the MIRI method was already established by the research team on the basis of agroclimatic data available between 1980 and 2011 in order to perform a water balance using the software CropWat version 8.0 (FAO). For conventional irrigation, the irrigation conditions of a commercial farmer were simulated. The CONTROL treatment irrigation was applied without restriction when water was available.

The same quantities and frequencies of application of fertiliser, insecticide, fungicide and herbicide products were applied on all three plots and between the two crop cycles.

3.2 The Aquacrop Model

The Aquacrop model uses different types of data in order to evaluate successively, and based on the previous step, the evolution of crop canopy cover, the crop transpiration using crop transpiration coefficient (KcTr) values, the biomass produced utilizing reference evapotranspiration (ETo) and finally the dry crop yield. The AquaCrop model's simulation of CC is one of its most significant features (Singh & al., 2013; Zeleke, 2019). Some of these steps can take into account the water, salinity, fertility, pollination and temperature stresses (Raes & al., 2018) (Fig. 3).

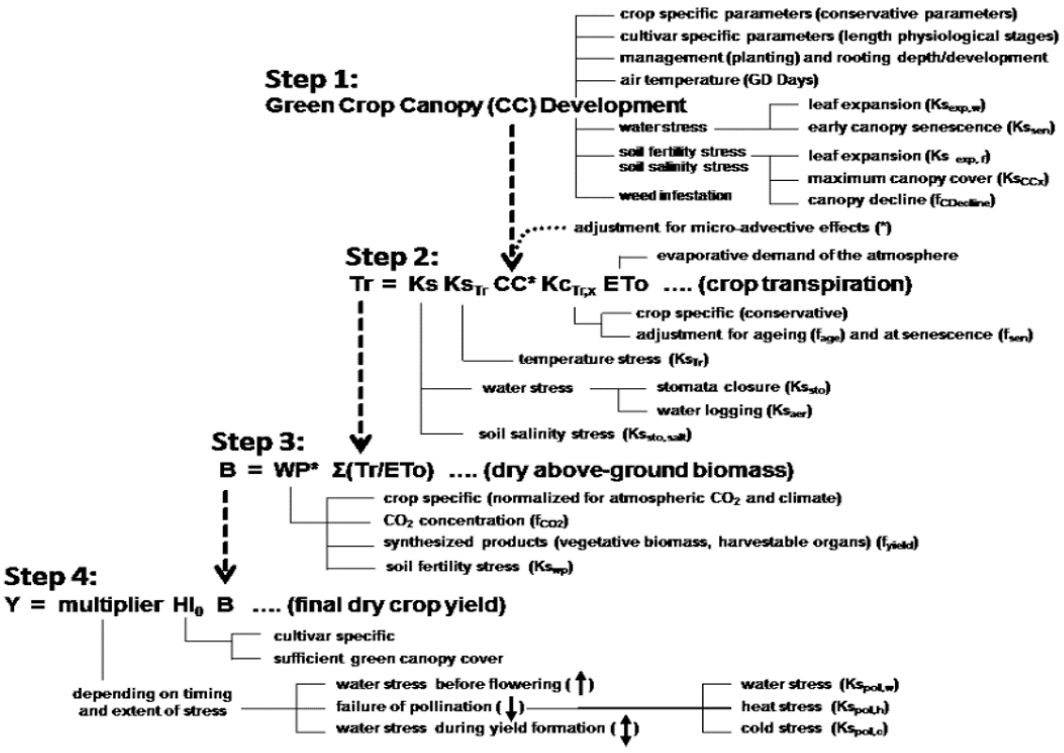

Figure 3: Description of the crop outputs calculation steps (Raes & al., 2018)

For each of these steps, the model requires vegetation crop parameters calibration, hydraulic and structure parameters of soil, climatic data (reference ET, maximal and minimal temperature, total precipitation) of the dates concerned, and data about the water table. To calibrate a vegetation file correctly in Aquacrop, several experiments are needed on different cycles, environments and fertilisations. For this reason, literature references dealing with studies on these traits in F67 (Appendix 8) were found to compare with the observed data.

3.2.1 Data collection for model evaluation

In a first step, the aim will be to evaluate with observed data the efficiency of the model in predicting the evolution of the canopy, its water productivity, dry yields and soil water content.

i Canopy cover

During these cycles, a quadcopter drone DJI Matrice 300RTK V2 was flown between 9 and 11 am bi-weekly from 30 days after sowing until senescence, and then weekly, to conduct the multi-temporal image acquisition stage. The capture of the aligned multispectral and thermal imagery was done with the Micasense Altum sensor. The Altum sensor has five multispectral bands (Red, Green, Blue, Red-Edge and NIR) and a LWIR thermal infrared, radiometrically calibrated. The information collected has a spatial resolution between 0.1 cm to 3.757 cm.

The canopy cover on each of the three plots was assessed for each measurement. Many techniques have already been used to evaluate the CC (Canopy Cover) from multispectral drone data. Among them, Machine Learning regression models such as random forest or ANN (Artificial Neural Network) give conclusive results (Niu & al., 2021). The random forest method was chosen.

Reflectances in the visible light length domains of rice remain relatively constant until leaf senescence when the plant stops photosynthesis (Gnyp & al., 2013) and these reflectances can vary with the amount of fertiliser applied; such as nitrogen (Gnyp & al., 2013). For this reason, a 20-point grid was generated over the entire plot on two dates per crop cycle, at the middle and end of the cycle on QGIS 3.24 with the "Pintmap" plugin. Through a supervised classification, the points were manually classified into the categories "Bare soil" and "Vegetation". 70 points were used as model calibration data and 30 as validation data to evaluate the model. The model calibration was performed on RStudio. The evaluation of the model on the validation data showed an Overall Accuracy of 100 %. The model was then applied to each of the three treatments for each measurement date via RStudio.

ii Dry crop yield and harvest index

For both cycles, dry yield was measured. First, the rice grains were harvested from four random areas of 1x1m per replication and block and weighed. The average moisture content per sample was measured with a device Mini GAC 2500 through dielectric permeability. Then, the mass of the grains was re-evaluated by adjusting the moisture content per grain to 14% by the formula 1, which is a moisture percentage value generally considered for dry grain (IRRI, 1994; Tirrol-Padre, 1995; Steduto & al., 2012).

$$14\%MC_{fw} = M \times \frac{(1 - 0,01 \times MC_{fw})}{0,86} \tag{1}$$

Where:
MC_{fw} = Moisture content on a fresh weight [%]
M = Mass of the grains [g]

An ANOVA on the yields observed on each plot was performed. Sixteen measurements were taken on each treatment per 1 m^2 area. Each sample was considered random, simple and the samples were considered independent. The Shapiro and Levene tests were applied for both cycles to validate the conditions of application of respect for the normality of the distribution of samples and equality of variances within each treatment. The table 1 shows the values of the ANOVA and the Post-Hoc tests. For Cycle 1, the ANOVA shows that there are no significant mean differences between the dry yields obtained per treatment. However, the null hypothesis that there are no "significant" differences between treatments can be discussed, as p-values greater than 0.05 could mean a small or weak difference between populations (Muff et al., 2022). The Post-Hoc test used to study the relationships between the different treatments one by one shows that there would be a possible small difference between the CONTROL treatment with both MIRI-AWD and MIRI treatments, with an adjusted p-value around 0.5, and no difference between the MIRI-AWD and MIRI treatments (Tab. 1). For cycle 2, the Post-Hoc test shows that there could be a significant difference between the MIRI-AWD and MIRI treatments with a p-value of 0.0624 and no difference between the other treatments. However, the detection of outliers shows that, contrary to cycle 1, there are four samples out of the 48 that deviate by 1.5 times the interquartile range on either side of the quartiles at 25% and 75% within their treatment, and that two values deviate by 3 times, considering these values as "outlier" and "extreme" respectively. A second ANOVA without these outliers shows that there would still be a moderate significant difference between MIRI-AWD and MIRI, and a strong significant difference between MIRI-AWD and CONTROL treatments with a p-value of 0.00428. Following these analyses, the dry yield results of the Aquacrop simulations were studied to assess whether they were able to meet the possible growth orders between the dry yield amounts of the different treatments, in addition to assessing the effectiveness of the simulations.

	CYCLE 1 (p-value=0,464)	CYCLE 2 (p-value=0,299)	CYCLE 2 without outliers (p-value=0,004)
MIRI-AWD x CONTROL	0,52	0,1	0,00428
MIRI-AWD x MIRI	0,999	0,0624	0,0288
CONTROL x MIRI	0,541	0,974	0,721

Table 1: p-values obtained by post-hoc tests between treatments and by ANOVA for each treatment

Harvest index (HI) is the weight of a harvested product as a percentage of the total plant weight of a crop (Dhital, 2011). HI were calculated by harvesting grains from four random areas of 25x25 cm per replication and block and then weighed wet and dry.

iii Soil water content

The soil moisture was measured with a TDR 350 moisture sensor at the same times than the others measures and to know if it was necessary to irrigate the MIRI plot. For the second cycle, a large part of the measurements were taken continuously via the Diviner tool. However, the recorded data is not available for technical reasons. Therefore, less data is available than for cycle 1.

3.2.2 Data collection for model calibration

i Vegetation indices

LAI is a dimensionless variable and a ratio of leaf area to per unit ground surface area (Myneni & al., 1995). Leaf area index (LAI) was determined with a ceptometer Accupar LP-80 (Metergroup,WA,USA) , according to the methodology described by Quevedo-Amaya & al. (2020). The LAI was assessed on the basis of leaf collection from four 25x25 cm samples per replication and treatment. According to Raes et al. (2018), this area is not sufficient and samples should be taken from areas of at least 1x1 m to have sufficiently representative samples. Moreover, the measured data show a relatively high variability (Fig. 6). Moreover, the biomass collected was only foliar and does not include the flowering, grain filling and ripening phases. These data were therefore not used for comparison with the data simulated by Aquacrop. However, they were used to try to draw additional conclusions about the phenology of rice through temporal evolution.

NDVI is defined as an indicator to determine the photosynthetic activity of a crop. Plants absorb energy from photons emitting in blue and red wavelength spectra to carry out photosynthesis and emit the excess energy as heat in the near infrared spectrum. The formula 2 quantifies the intensity of photosynthesis between 0 and 1 (Myneni & al., 1995). The data measured by the drone made it possible to calculate and use the NDVI at a height of 60 m. The advantage of NDVI is that it can discriminate between different phenological stages such as tillering, heading/flowering and maturation (Wang & al., 2014, Zhang & al., 2017).

$$NDVI = \frac{NIR - Red}{NIR + Red} \tag{2}$$

Where:

NIR= Near infrared pixel value
Red = Red pixel value

These data will allow an in-depth study of the values needed to calibrate the phenology of the F67 variety (Wang, 2014; Raes & al., 2018).

3.2.3 Crop parameters calibration

All the crop parameters are listed in the appendix 8 and can be:

- **Conservative crop parameters** which do not change substantially with time, management practices, geographic location or climate. They are also assumed not to change with cultivars unless shown otherwise (Raes & al., 2018). They are already calibrated and provided in the literature related to Aquacrop (Steduto& al., 2012).

- **Cultivar specific and non-conservative parameters** which might require an adjustment when selecting a cultivar different from the one considered for crop calibration (through plant breeding and biotechnology), or when the environmental conditions differ from the conditions assumed at calibration (field management and conditions in the soil profile) or when the planting method is altered. These parameters are the most important for the calibration of Aquacrop, especially the phenology which can vary a lot depending on the environment and the varieties (Raes & al., 2018).

The rice *Oryza sativa* L. variety concerned is called Fedearroz 67 (F67). All the management and cultivar parameters were studied to try to calibrate them according to the the experiments and literature when data were missing or not completely reliable.

i Management parameters

1. **Plant density :**

   - Sowing rate cycle 1: 170 kg/ha
   - Sowing rate cycle 2: 150 kg/ha
   - Seed weight: 28 mg/1000 seed, according to the observations of the two cycles and Tirado & al. (2017)

   ⇒ Plant density calculation

2. **Maximal canopy cover**

   The maximal canopy cover varies with crop type but it is also determined by planting density and can varies between 75% and 100% (Raes & al., 2018). The data calculated thanks to the supervised classification with the remote sensing allowed to consider a maximal value around 99 % (Fig. 4).

3. **Time to reach 90% seedling emergence**

   It's affected by field preparation and soil temperature. Because of field preparation, soil temperature and water content vary with each case, the time to emergence is user specific (& al., 2018). The value is set at 10 days, based on the litterature (Herrera Vidal, 2020 ; Burgos Bedoya, 2021, Gomezcasseres Argumedo, 2021).

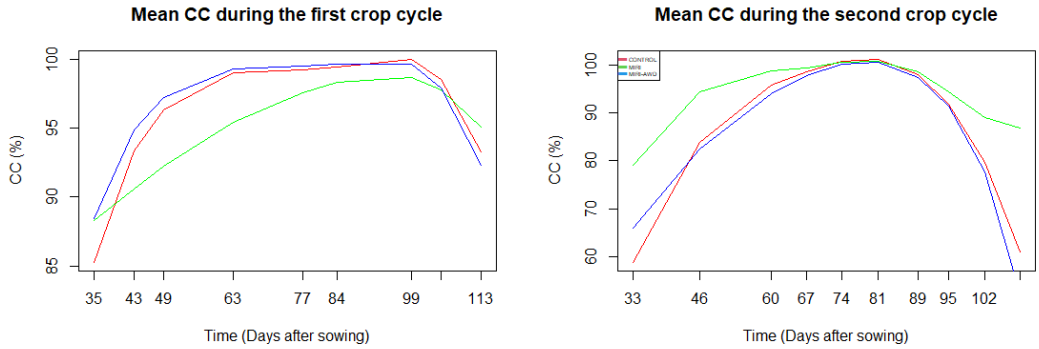

(a) Cycle 1

(b) Cycle 2

Figure 4: Mean canopy cover for the three treatments accross the time for the two crop cycles

ii Cultivar parameters

1. Root system

- Minimum root depth: 15 cm
  - Considering the depth of sowing (3-5 cm with mechanical seed drill) + 10 cm for the emergence
  - 15 cm at emergence after 10 days (Granados, 2021)
  - 15 cm for annual crop (Allen & al., 1998)
- Maximum root depth: 30 cm
  - 20-30 cm for F67 (Tirado & Castilla Lozano, 2017 ; SATREPS,2019 ; Granados, 2021)
  - 50 cm - 1 m for *Oryza sativa* L. (Allen & al., 1998)
  - 20-40 cm for others *Oryza sativa* L. varieties (Price & al., 1997)

There is a high genetic variation in rooting patterns in rice (O'Toole & Bland, 1987). Soil penetration resistance, and hence root depth, is related to texture, structure, dry bulk density, soil water content and organic matter content (Marshall & al., 1996). Rice crops have often a compacted layer at 30-40cm due to the passage of machines (Tirado & Castilla Lozano, 2017). An excavation on the experimental plot showed that the soil was much more compacted between 40 cm and 50 cm deep. The increased levels of root depth are seen in soils without extensive layering or other rooting depth-restricting properties. The FAO lower value can be used to schedule irrigation (Allen & al., 1998). The considered value of maximal root depth was 30 cm.

2. Soil water content at anaerobiotic point

It's defined as the value between the field capacity and the saturation when a anoxic stress occurs. The default value for the rice is 0 % (Steduto & al., 2012). Indeed rice has aerenchyma allowing it to capture oxygen from outside the soil in times of waterlogging. To undergo stress, it must remain underwater for several weeks, which is not the case here (Miro & Ismail, 2013).

3. **Salinity stress**

When salt stress occurs, the rice plant may find it more difficult to take up water due to osmotic pressure from a soil conductivity of 3 dS/m (Steduto & al., 2009). A measurement in soil/water suspension ratio 1:5 (weight/volume) was carried out to assess the conductivity of the three plots, which is 0.2 dS/m for all three. Moreover, three conductivity measurements of the water irrigation made with a conductivity meter were the same value of 0,263 dS/m, and the soil is well drained with a 60% sand texture. Then, the choice was to no take into account the salinity stress since the conductivity is fifteen times smaller than the stress threshold and could not increase.

4. **Harvest index**

Harvest Index values generally vary widely between cultivars, locations, seasons, fertility management and ecosystems, ranging from 0,35 to 0,62 for upland rices (Fageria, 2007). HI of modern, short-duration tropical cultivars is about 0,35 to 0,4 in the wet season and 0,45 to 0,5 (45 to 50 percent) in the dry season (Steduto & al., 2012). For Aquacrop, the harvest index need to be calibrated without water stress because it's reevaluated according to the water stresses during the simulation (Raes & al.,2018). The rice harvest index values reached in the tropics is 0,5 (Sheehy & Mitchell, 2013). Due to plant breeding and biotechnology, HIo is likely to increase in the future (Raes & al.,2018). The mean value observed of the first cycle (0,47) is reliable in comparison of cited values but inconsistant with the values of the second cycle (>0,6). Moreover, there were much more water stresses during the second cycle due to works on irrigation canals. The value of 0,47 is kepped and is near to the values between 0,42 and 0,44 that have been already get for F67 (Heros & al., 2022).

5. **Phenological periods**

Aquacrop considers temperature as an internal clock for rice development. For the Growing Degree-Day mode, the number of calendar days can be calibrated in growing degrees per day, representing the difference between the average daily temperature and the default temperature for the crop under which there would be no further rice growth (Raes & al., 2018). This mode then allows the study of the development of the plant in other years according to the climate observed at that time. Only the observed data for the first cycle were used to calibrate the phenological stages in order to observe the efficiency of estimating the evolution of the simulated canopy cover for the second cycle. The values assessed in days were then transformed into Growing Degree Days by the software.

The first cycle observed duration for reaching the maximum elongation of the internodes, considered as the maximal canopy cover value, is at around 60 DAS (Fig. 4). According to FEDEARROZ (2022), the F67 variety reaches the maximum internode development between around 60-70 days. It is important to know that the canopy is defined as the aboveground portion of a plant cropping or crop, formed by the collection of individual plant crowns (Campbell & al., 1989). Although the number of tillers starts to decrease during panicle initiation, the tillers and leaves on the tillers continue to grow and the internodes widen, leading to a lower rate of increase in LAI and CC by taking into account the panicle growth. The coverage increases further after at minus 2%, but taking the first values close to 100% seems more recommendable given the small increase over a relatively long period of time. Aquacrop still considers also a few additional cover

percentages of 2% after the fixed canopy cover date, thanks to the mode "Determinancy linked flowering" to consider this phenomenon. This value is only used to calculate the Canopy Growth Coefficient in the software, which has been evaluated at 12%/day, representing the percentage of canopy growth per day or per Growing Degree Day and is not recorded in the external crop file.

The evolution of NDVI values during a crop cycle increases during the tillering phase, stagnates during the vegetative lag period, then increases again, with a decreasing growth rate per day, during panicle development until a maximum value representing flowering. The observed drone data of the two cycles show a first decrease in NDVI (Fig. 5) at around 77 and 60 days from the higher NDVI value, and correspond more or less to others measurements on F67 flowering (Herrera Vidal, 2020 ; Burgos Bedoya, 2021) and maximal NDVI moment(Lozano & Ospina, 2019). The maximal values of the LAI (Fageria, 2007) and the NDVI (Wang & al., 2014; Zheng & al., 2017) values are supposed to be reached at flowering time (Fig. 6). The value of 75 days is chosen for the flowering time beginning. Shortly after, the leaves begin to wilt and yellow causing the senescence (Fageria, 2007), and the spikelets stand upright and remain green during the milking and doughing phases, slowing the decrease in NDVI due to the senescence (Wang & al., 2014). The midpoints of the periods between the time of maximum LAI and the next date were averaged, a number of days of 85 was set for the senescence period, occuring often more or less ten days after the heading or flowering date, after the beginning of milk phase (Zheng & al, 2017; Benitez, 2020). The grains of *Indica* varieties of *Oriza Sativa* L. fill up to 25 to 35 maximum after flowering in the tropics (Jennings, 1979; Steduto & al., 2012), and then the maturity phase is reached. From this maturation time, they become white-yellow and the NDVI decreases even more strongly (Reed & al., 1994; Wang & al., 2014) around from 110 days for the cycle 1. The chosen value for the maturation time is 110 days, but is slightly superior with the litterature values (Herrera Vidal, 2020 ; Burgos Bedoya, 2021). The maximum root depth is reached around the time of flowering (Fageria, 2007). Hence, the value has been set at 70 days. These values, although relatively arbitrary, may still be discussed. Indeed, Figure 4a. shows that the canopy starts to decrease later. Aquacrop considers that the simulation stops at maturity, although harvesting has taken place beyond 120 days. However, it is recommended that the ripening DAS should not necessarily be set on the day of harvest (Raes & al., 2018). The LAI, NDVI and CC measurements for cycle 1 show that senescence decays relatively slowly over time. The Canopy Decline Coefficient, describing the percentage decline per Growing-Degree day between senescence and maturity days, was manually adjusted with Cycle 1 data to 4.2%/day, or 0.236 %/GDD.

For the duration of the flowering period, it was estimated at 13 days based on values of other varieties studied in Colombia or under the tropics in arid climate (Fernandez, 2013 ; Melo Solarte,

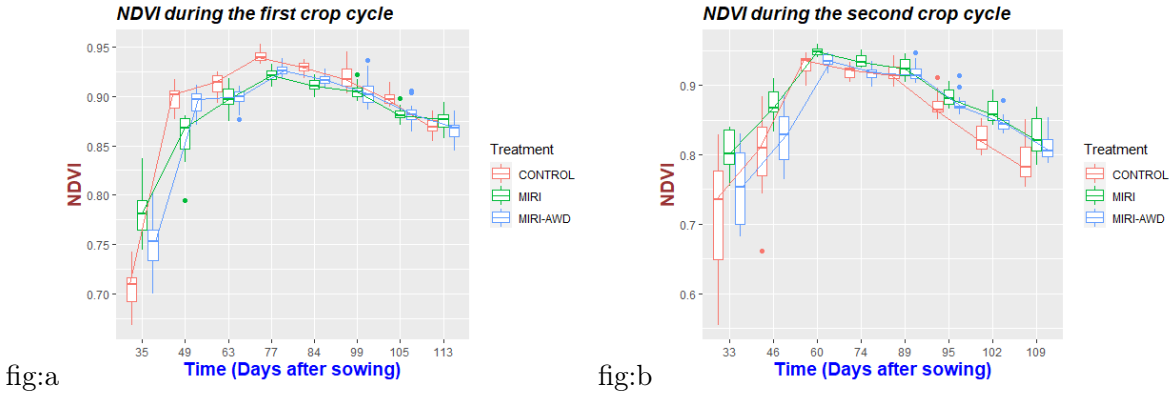

fig:a (a) Cycle 1

fig:b (b) Cycle 2

Figure 5: NDVI Boxplots for the three treatments accross the time for the two crop cycles

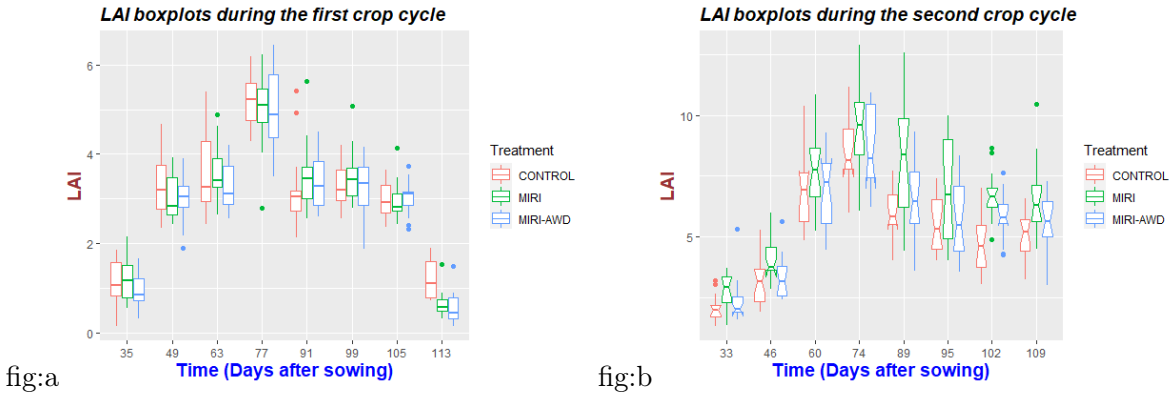

fig:a (a) Cycle 1

fig:b (b) Cycle 2

Figure 6: LAI Boxplots for the three treatments accross the time for the two crop cycles

2019). According to Steduto & al. (2012), this value is less than 15 days in the tropics.

6. **Fertility stress**

Fertility stresses influence canopy development. These are parameters to be calibrated for each specific case. It requires access to observed green Canopy Cover (CC) and biomass production (B) in two well watered fields: one with and the other without soil fertility stress (Raes & al., 2018). This was not possible in these studies, they will therefore not be considered.

3.2.4 Soil parameters calibration

1. **Soil layers**

Texture percentages were obtained using the Bouyoucos method and the percentage of organic matter by the Walkley and Black method with three samples of 15 cm deep per experimental plot (Table 3). The "General Soil Survey and Land Zonification of Tolima" (IGAC, 2004) includes soil descriptions and mapping in the Tolima region. The map was clipped using QGIS 3.24 to the boundaries of the experimental area. Three soils, classified according to the USDA classification

(USDA, 2014), were likely to be present. The "Typic Haplustolls" corresponds to the textural data and the description (Table 2). Its textural data was used for the lower layers that were not studied.

An excavation on the experimental plot showed a distinct layer much more compacted between 40 cm and 50 cm deep and a very loosely compacted sandy layer underneath. The soil layers in Aquacrop were separated between 0-40 cm, 40-55 cm and 55-160 cm respectively for the A layer studied with experimental data, the more compacted layer and the sandy layer. Organic matter and textural data of Bw and C layers (IGAC, 2015) were used for the two last layers. Taking the lower layers into account allows better consideration of capillary rise and deep percolation.

Horizon		**Granulometry**				
Depth (cm)	Layer	Sand (%)	Silt (%)	Clay(%)	Organic Carbon(%)	Organic Matter (%)
0-30	A	74	16	10	0,61	1,05
30-58	Bw	78	12	10	0,22	0,38
58-120	C	82	12	6	0,22	0,38

Table 2: Literary values used for the soil of the experimental plot

2. **Conductivity and retention curve values**

The retention values were obtained using the pressure plate method (Table 3). The soils are of the "Sandy Loam" type according to the USDA classification. The achievable retention curve values seem to be far too high compared to the reference values, which are maximum 15% for the wilting point (Allen & al., 1998). The latter seems to be far too high. However, these are paddy soils, which are the largest anthropogenic wetlands and are Anthrosols created by puddling the wet soil (Lal, 2021). In these soils, the structure is sometimes severely altered as a result of constant ploughing or disking to the same depth, allowing equipment traffic, especially on wet soils, the using of a limited crop rotation without variability in root structure or rooting depth, and the using of heavy equipment for construction site preparation or land levelling (Raes & al., 2018), which are practices used here for the sowing and the crop preparation in MIRI. Sand, sandy loam, sandy clay loam, and clay soils all have decreased hydraulic conductivity, non-capillary pores, and void ratios as a result of compaction treatments and the micropores grew at the expense of macropores during compaction and hydraulic conductivity was directly connected to the macropore space (Ghildyal & Satyanarayana, 1965), decreasing the total available water for plants. Repeated addition of organic matter and NPK fertilisers can also increase the retention curve values on paddy soils (Liu & al.,2011; Lu & al., 2019). But here the analyses show that in the soils these components have medium to low concentrations. Hence, the desicion was made to keep the retention curve values.

The saturation conductivity (Ks) of the soil was estimated experimentally by Philip's infiltration equation (Philip, 1957), based on measurements made with a double-ring infiltrometer. The measurements appear to be very different between the three plots, ranging from 144 to 1162 mm/-day. These measurements are known to be very heterogeneous in crop soils (Ahuja & al., 1989). The conductivity, permeability, and diffusivity of water and air could be all impacted by soil compaction since it increased the bulk density and strength of the soil (Greenland, 1977). Hydraulic conductivity underneath permanent tracks in a controlled traffic system spreaded laterally into

the subsoil (Kirchhof et al., 2000). The values therefore do not seem to be representative of the average Ks present. On the other hand, Shwetha & Varija (2015) demonstrated that saturation conductivity could vary from 278 to 2474 mm/day for a sandy loam agricultural soil. The Saxton model (Saxton, 1986), recommended by the Aquacrop user manual for modelling missing values (Raes et al., 2018), was used to replace them. These values appear to be more consistent with reference values provided in the literature for this soil type (Allen et al., 1998) and are included in the table 3.

Analytical determination	**Values**	**Conductivity-Retention values**	**Values**
CONTROL/MIRI			
Sand percentage (g/100g)	66,45	Permanent wilting point (g/100cm^3)	23,53
Clay percentage (g/100g)	15,43	Field capacity (g/100cm^3)	28,92
Silt percentage (g/100g)	18,12	Saturation (g/100cm^3)	45,53
Organic matter (g/100g)	2,33	Conductivity at saturation measured (mm/day)	1162
		Conductivity at saturation modeled (mm/day)	1200
MIRI/MIRI-AWD			
Sand percentage (g/100g)	68,46	Permanent wilting point (g/100cm^3)	25,83
Clay percentage (g/100g)	13,41	Field capacity (g/100cm^3)	29,62
Silt percentage (g/100g)	18,13	Saturation (g/100cm^3)	49,40
Organic matter (g/100g)	3,10	Conductivity at saturation measured (mm/day)	144
		Conductivity at saturation modeled (mm/day)	902
MIRI-AWD/CONTROL			
Sand percentage (g/100g)	67,09	Permanent wilting point (g/100cm^3)	28,00
Clay percentage (g/100g)	13,99	Field capacity (g/100cm^3)	32,18
Silt percentage (g/100g)	18,92	Saturation (g/100cm^3)	47,66
Organic matter (g/100g)	2,71	Conductivity at saturation measured (mm/day)	350
		Conductivity at saturation modeled (mm/day)	958

Table 3: Analytical composition and retention-conduction values of the three irrigation plots

For deeper layers, conductivity curve (K_{sat}) and retention curve (water content of PWP, WP and Sat) values were simulated using the model of Saxton with SPAW software as previously. The organic matter rate was determined using organic carbon multiplied by a factor of 1,724 (Nelson & Sommers, 1996).

3. **Runoff and deep percolation**

The Curve Number of a soil is a function of its type, slope, land use, cover and the relative wetness of the top soil (Raes & al.,2018) and is an empirical parameter used in hydrology for predicting direct runoff or infiltration from rainfall excess. Its value varies from 30 to 100, low values imply more infiltration and high values more runoff (USDA, 2004). Its base value was set at 46, corresponding to a soil with a saturation conductivity of more than 864 mm/day. This figure is set for a slope of 5 %, corresponding to the longitudinal slope measured in the field. The crop type "Row Crop, Straight Row" was selected, with the mode "Poor" based on soil retention

curve measurements and farming practices, increasing the Curve Number (USDA, 2004; Raes & al., 2018).

4. **Penetrability**

The bulk density of the first 15 cm of soil averages 1.55 g/cm^3, close to the value of 1.63 g/cm^3 for a sandy loam that may cause a barrier to root growth according to Raes & al. (2018). The value was set at 62 %, which is the percentage difference between the ideal bulk density and the value that restricts root development according to Raes & al (2018).

As mentioned in the point 3.2.3, these crops have often a compacted layer at 30-40 cm due to the passage of machines (Tirado & Castilla Lozano, 2017). The distinct layer may be a hardpan, formed by deposits in the soil that fuse and bind the soil particles. Hardpans limits or inhibited the expansion of the root zone and are also largely impervious to water. A restrictive soil layer may also be the result of soil compaction which increases its bulk density (Raes & al. ,2018). This may happen because of the agricultural practices used and mentioned in 3.2.3. An excavation on the experimental plot showed a distinct layer much more compacted between 40 cm and 50 cm deep, appearing to be a hardpan, and a very loosely compacted sandy layer underneath. The decision was made to set the penetrability arbitrarily at 10 % for the hardpan layer between 40 and 55 cm.

5. **Stoniness**

After excavation, measurements of the mass percentage of stone (i.e. diameter particle $>$ 2 mm) in the different horizons were measured using the formula 3 and fixed in Aquacrop. Stoniness influences the TAW (Raes & al., 2018). The percentages showed about 10% for layer A and 30% for layer Bw.

$$Mass\%_{gravel} = 100\frac{m_{gravel}}{m_{gravel} + m_{finesoil}} \tag{3}$$

3.2.5 Climatic data

The Climatic data needed for Aquacrop are total precipitation, maximum temperature, minimum temperature and FAO Pennman-Montheit formula of reference daily evapotranspiration. The FAO Penman-Montheit formula of reference evapotranspiration was used (Eq. 4) allowing to calculate the daily height of water in millimeters evapotranspirated by square meter of grass of 0,12 m uniform height, a fixed canopy resistance of 70 s/m and an albedo of 0,23 with the assumption that there is no water stress after extensive testing of different formulas among physically-based equations by the FAO (Pereira & al., 1996; Allen & al., 1998).

The required climatic data were extracted from the agroclimatic station of the Nataïma research centre. No hourly data were missing for the simulation periods studied, allowing the daily values to be calculated. Moreover, no outliers outside 3 times the standard deviations around the mean were detected (Sarmad, 2006). The package "Sirad" was used on RStudio to apply the formula 4 at each day. The saturation vapor pressure was obtained thanks to the Magnus formula (Eq. 5) and allowed to calculate the mean ambient vapor pressure thanks to the equation 6. The sensible heat flux into the soil at a daily scale can be neglected and the psychrometric constant were calculated with the equation 7 (Allen & al., 1998).

$$ET_0 = \frac{0.408\Delta(R_n - G) + \gamma\frac{900}{T+273}u_2(e_s - e_a)}{\Delta + \gamma(1 + 0.34u_2)} \tag{4}$$

Where:

ET_0 = Reference evapotranspiration $[mm.day^{-1}]$
Rn = Net Radiation Flux $[MJ.m^{-2}.day^{-1}]$
G = Sensible heat flux into the soil $[MJ.m^{-2}.day^{-1}]$
e_s = Mean saturation vapour pressure $[kPa]$
e_a = Mean ambient vapour pressure $[kPa]$
γ = Psychrometric constant $[kPa.^{\circ}C^{-1}]$
Δ = First derivative of the vapor pressure-temperature function $[kPa.^{\circ}C^{-1}]$
T = Daily mean air temperature at 2m height $[^{\circ}C]$
u_2 = Daily mean wind velocity at 2m height $[m.s^{-1}]$

$$\begin{cases} e_{sM} = \frac{0.6108*exp(17.27*T_{max})}{T_{max}+237.2} \\ e_{sm} = \frac{0.6108*exp(17.27*T_{min})}{T_{min}+237.2} \end{cases} \tag{5}$$

$$e_a = \frac{RH}{100 * ((e_{sM} + e_{sm})/2)} \tag{6}$$

Where:

e_{sM}= Maximal saturation vapour pressure $[kPa]$
e_{sm}= Miminal saturation vapour pressure $[kPa]$
e_a= Mean ambient vapour pressure $[kPa]$

$$\gamma = \frac{c_P P}{\epsilon\lambda} = 0,665 \times 10^{-3} P = 101,3(\frac{293 - 0,0065z}{293})^{5,26} \tag{7}$$

Where:

γ= Psychrometric constant $[kPa.C^{-1}]$
P= Atmospheric pressure $[kPa]$
λ= Latent heat of vaporization, 2.45 $[MJ.kg^{-1}]$
c_p= Specific heat at constant pressure, 1.013×10^{-3} $[MJ.kg^{-1}.C^{-1}]$
ϵ= Ratio molecular weight of water vapour/dry air, 0.622

3.2.6 Irrigation

The flow rate was measured using a Parshall flume, an ultra sonic sensor to measure the inlet water level. The water level was converted to flow rate using a regression equation. The amount of water was calculated by multiplying the average flow rate by the irrigation duration. The applied irrigation height was then calculated by dividing the average flow rate by the plot area. This allowed the irrigation schedule of the three plots for both crop cycles. Aquacrop uses net irrigation, i.e. the amount of irrigation only applied in the field. However, output water was not measured, as plots were irrigated to fill 80 % of the crop area in order to reduce water losses. In addition, the longitudinal slope of the land was only 3 %.

The wetted surface was set at 100 %. As mentioned on the page 23, the conductivity of the water measured is 0.263 dS/m. Moreover, the conductivity measured near Nataima in the literature is always lower than 0.5 dS/m (Cardenas Lopez & Romero Perdomo, 2017), considered as a safety value water conductivity for crops (Raes & al., 2018). This is because the water is treated and the sediments are extracted before entering in the irrigation district.

The simulations were based on a saturated soil water content at sowing, as achieved in the field.

3.2.7 Water table

Excavation of a hole allowed us to estimate the depth of the water table at 1.60 m, this influences the water content in the soil through capillary rise (Raes & al., 2018). Since the soil has good drainage, this information may decrease the magnitude of simulated stresses that could be overestimated since virtually no stress would have been detected during the first crop cycle.

3.3 Sensitivity analysis

3.3.1 Method description

i Morris sensitivity analysis

The Morris sensitivity analysis is used here. It is a "one at a time" sensitivity analysis method, where only one parameter is changed in each simulation. The variation of the objective function F with respect to a parameter X_i is calculated by finite difference between two sets of identical parameters except for one (Fig. 4).

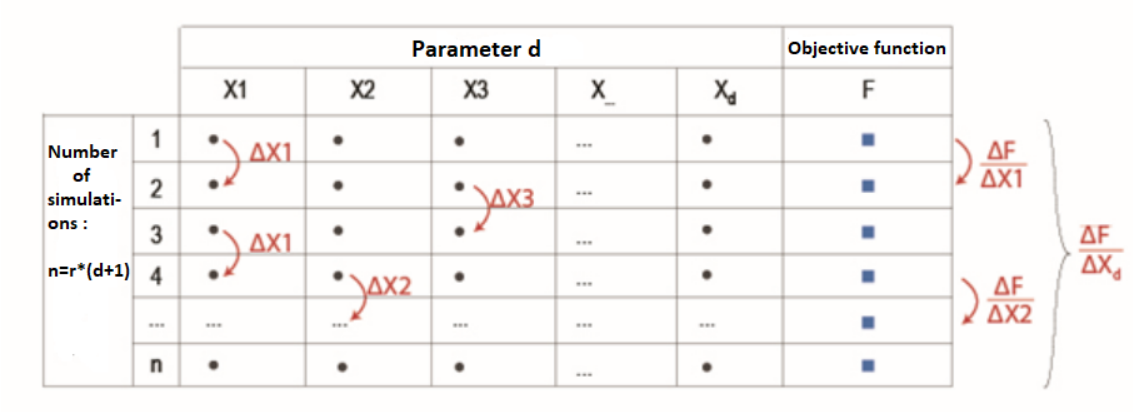

Figure 7: Table showing the modification of a different parameter at each repetition of the simulation (from Taupin 2018)

Each interval defined for each parameter is divided into q equidistant levels defined. A value of one level of each parameter is randomly selected, and then the value of each parameter is successively varied one at a time to measure the impact on the output function F. This same step is repeated a number of times, each time taking a new starting data set. This number of repetitions is called the number of "trajectories". The number of trajectories should be selected to cover the distribution of parameter values in space (Campolongo et al., 2007). A number of trajectories of 100 is sufficient for this type of exercise on Aquacrop with a similar number of input parameters (Vanuytrecht & al., 2014; Coudron & al., 2021) and the recommanded level number is $q = 8$ (Vanuytrecht & al., 2014). In total, therefore, $n = r \times (d + 1)$ simulations will have been performed.

At each variation Δ_{ij} of parameter x_i within a trajectory j, the difference caused in output function f, representing the value of an output variable of interest, is divided by Δ_{ij}. This allows the importance of the variation Δ_{ij} on f to be estimated by obtaining the elementary effect vectors EE_{ijklm} (Eq. 4).

$$EE_{ijklm} = \frac{f(X_k, X_l, X_m, x_{1j}, ..., x_{ij} + \Delta_{ij}, ..., x_{pj}) - f(X_k, X_l, X_m, x_{1j}, ..., x_{ij}, ..., x_{pj})}{\Delta_{ij}} \tag{8}$$

The simulations create elementary effect vector values EE_{ijklm} for each of the six output variables by each of the 116 simulation days each input parameter within each trajectory in different climatic and soil environments and years. The number of days corresponds more or less to a classical cycle duration, between may and septembre. Each of these combinations exists by combination of soil types m, years l and climates k with X_m, the soil parameter values, X_l the years, and X_k the climates variables respectively. The total simulation number is equal to : 100 trajectories $\times$ 4 soils in the first climatic zone $\times$ 11 soils in the second climatic zone $\times$ (29+1) parameters $\times$ 116 days = 8578200. The 5 output variables studied are CC, biomass, dry yield and soil moisture content at 20 and 40 cm.

Then, the series of elementary effects $\frac{\Delta F}{X_i}$ of each parameter is treated in order to calculate an absolute average elementary effect μ^* and a standard deviation σ (Morris, 1991; Campolongo, 2007). The distribution mean of the absolute values of the elementary effects solves the problem of the effects of opposite signs occuring when the model is non-monotonic (Campolongo, 2007).

The analysis was then carried out on RStudio by implementing the "Aquacrop plugin" to be executed in loops. The "Sensitivity" package was used to apply the Morris function.

ii Screen parameter effects

These elementary effect vectors have to be rescaled in order to make the influence of the input parameters on the outputs comparable and representable. Indeed, as the ranges of values defined for each parameter are relatively different, they need to be scaled so that they can be represented and compared in relative terms (Brun & al, 2001). For this purpose, the ratios of the standard deviations of the values of the intervals of each input parameter and the standard deviations of the values of the output variables were multiplied by the elementary effect vectors (Eq. 9) (Sin & al., 2009).

$$EE^{scale}_{ijklm} = \frac{\sigma_{xi}}{\sigma_{fouput}} \times EE_{ijklm} \tag{9}$$

3.3.2 Input parameters and values selection

i Crops values

The selection of crop parameters are listed in the table 4. The ranges of some parameters, mainly non-conservative, are based on the literature, using the values quoted for varieties present in the trop-

ics, as locally as possible, in upland rice crops. The ranges of other parameters, mainly conservative, are based either on the limits of the values admitted by Aquacrop, or on an arbitrary choice of the limits of the ranges of values that may seem coherent.

In order to remain within the simulation of plausible scenarios, some phenological stages were defined by varying a number of days after the maximum canopy. This is the case for the duration between the time to reach maximum canopy cover and flowering and maturation. Because of this definition, some inputs influence other inputs, providing a disproportionate effect that is not representative of the variation of the parameter alone. This would require varying each input at a fixed value of the variable causing the variation in the other inputs. However, this aspect was neglected due to the high computational time and the high number of 100 value trajectories divided into eight levels within relatively short intervals for those phenological variables that are counted as integer values, assuming that the defined trajectories and levels can realise enough possible combinations between the inputs to cover the whole domain. In addition, the time parameter required to reach maximum coverage was not taken into account in the analysis of the results, as it provides a cumulative effect on the outputs through its influence on the other inputs.

Crop Parameter	**Variable Name**	**Chosen interval**	**Source**
Stress			
Soil water threshold for canopy expansion (%RAW) - Upper threshold	canup	0-5	
Soil water threshold for canopy expansion (%RAW) - Low threshold	canlow	35-45	
Soil water threshold for stomatal closure (%RAW)	ssto	40-50	
Shape factor for water stress coefficient for canopy expansion	scan_shp	1,5-5,5	
Shape factor for water stress coefficient for stomatal control	sstom_shp	1,5-5,5	
Shape factor for water stress coefficient for canopy senescence	ssen_shp	1,5-5,5	
Maximal temperature stress for pollinisation (°C)	polup	35-40	Fageria, 2007 Kropff and al., 1994
Minimal temperature stress for pollinisation (°C)	polmin	8-20	Kropff and al., 1994
Canopy			
Max canopy cover (%)	maxcnp	90-100	
Initial leaf area at emergence (cm^2/plant)	leafini	2,5-3	
Canopy decline coefficient (%/day)	cdc	7-11	
Depth development			
Max effective rooting depth (m)	maxroot	0,20-0,40	
Min effective rooting depth (m)	minroot	0,10-0,15	
Shape factor describing root zone expansion	root_shp	15-45	
Maximum root water extraction in top quarter of root zone ($m^3/m^{-3}*day^{-1}$)	maxext	0,03-0,06	
Maximum root water extraction in bottom quarter of root zone ($m^3/m^{-3}*day^{-1}$)	minext	0,01-0,03	

Crop Parameter	Variable Name	Chosen interval	Source
Cultural coefficient			
HI (%)	hi	40-50	Steduto and al., 2012
Transpiration coefficient (Kc Tr)	kc	1,05-1,2	Allen and al., 1998
Water productivity (g/m^2)	wp	17-19	Melo Solarte, 2019
Decline of crop coefficient (% of CCx per day) as a result of ageing, nitrogen deficiency	kcdec	0,075-0,225	
Possible increasing HI (%)	hiinc	5-15	Steduto and al., 2012
Stade length		Fageria, 2007 ; Steduto and al., 2012 ; Melo Solarte, 2019 ; Herrera Vidal, 2020 Burgos Bedoya, 2021 ; Gomezcasseres Argumedo, 2021	
Time from sowing to emergence (days) or recovery (from transplanted seedlings)	sini	5-15	
Until maximal canopy cover (days)	smax	55-70	
Canopy growth coefficient (%/day)	cgc	$\frac{-ln(\frac{2*CCo}{0,25*(CCx^2)})}{DayCCx}$	
After maximal canopy until flowering (days)	sflow	7-15	
After maximal canopy until senescence (days)	ssen	15-23	
Flowering length (days)	lflow	10-15	
After maximal canopy until maturation (days)	smat	30-40	
HI length (days)	lhi	15-20	
Until maximal rooting depth (days)	sroot	60-80	

Table 4: Chosen intervals of the retained crop parameters for the Morris sensitivity analysis

ii Climatic values

1. **Climatic description of Tolima and measured data acquisition**

The region of Tolima is a valley between two mountain ranges where the topography varies a lot, and hence where some climatic variables mean on a period may significantly change. According to the IDEAM (2018), the rice crops land use plots, classified according to the Land Use Land Cover CORINE classification, are divided between two types of climate. The crossing of the CORINE classification and the Caldas-Lang climatic classification of the IDEAM (2014) made with QGIS 3.24 shows that 23% rice crops are in a tropical "Warm semi-humid" climate, with an average annual temperature between 22,8°C and 25,8°C and an average annual precipitation between 1500-2500 and 1051 mm, and 77% are in a tropical "Warm semi-arid" climate, with an average annual temperature between 27 and 30°C and an average annual precipitation between 1000 and 1500 mm (IDEAM, 2018) (Fig. 8). It is interesting to take into account in these simulations the crops present in these regions since the climate varying according to the topography can have an impact on the development of the crop (Dutta & al., 1996).

Based on this classification, it is assumed that the annual means of the required climatic data are relatively similar between the ranges of values of climatic variables defined for these classes, although the topographic variability is significant in this region and implies some variability within these areas (Fig. 8 b). The data have been taken in the database of one station in the semi-arid region and another in the semi-humid region (Fig. 8 a) between 2005 and 2022 for reasons of availability. According to the FAO, when wind speed values are missing, data from the nearest station could be used if the air masses have the same origin, and similar maximum

and minimum relative humidities observed (Allen & al., 2018). Data from the semi-arid station were used for the not found values for the semi-humid station as the air masses passing through these locations are generally from the south and have similar ranges. Since some of the values are available by hour, and the solar radiation evolution across the time has a sinusoïdal form with maximal values at midday, the solar radiation by day shouldn't be evaluated when there are missing values during the day. The day duration, between the sunrise and the sunset, varies relatively little (30 minutes) between the equinoxes, near the Equator (sunrise-and-sunset, 2022). Only the days with values between 7 A.M and 5 P.M were kepped, i.e the hours where the values were generally different of zero. Some luminance values over 5 years, i.e the fraction of solar luminance by day, were used in order to improve the estimations of the solar radiation since there is a high correlation between them and it is generally employed for the solar radiation estimations (Angström, 1924; Prescott, 1940). Then, all the others outliers of variables outside of 3 times the standard deviation from the mean were deleted (Sarmad, 2006).

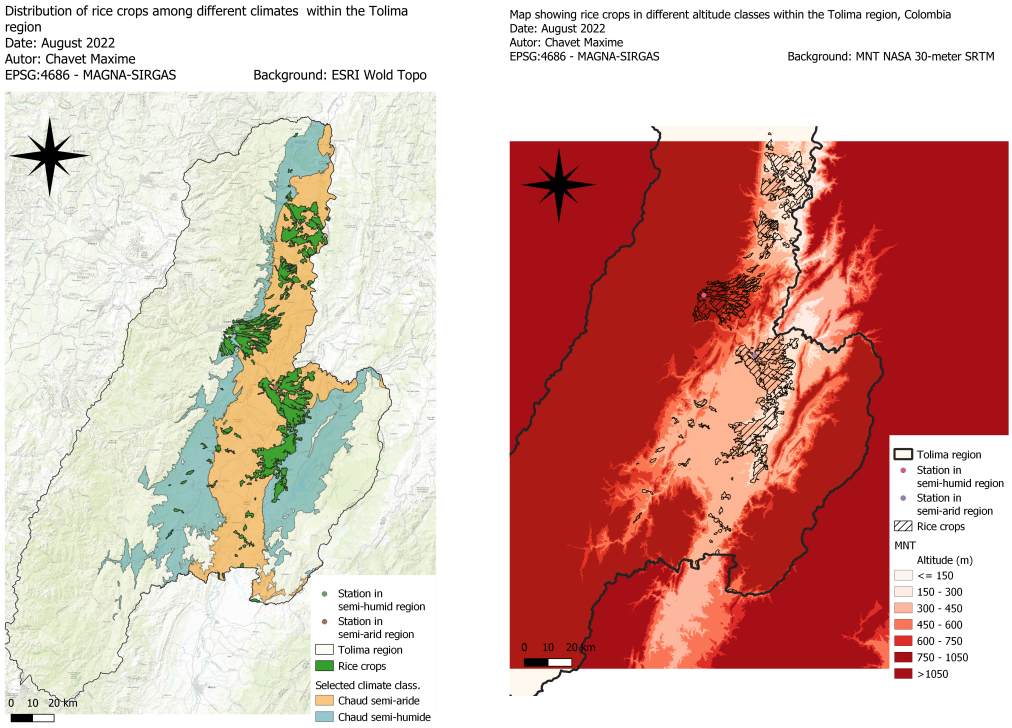

(a) Distribution of rice crops (IDEAM, 2018) among different climates (IDEAM, 2014) within the Tolima region, Colombia

(b) Distribution of rice crops (IDEAM, 2018) among different altitude ranges (NASA, 2022) within the Tolima region, Colombia

Figure 8: Maps showing the distribution of rice cultivation areas within the Tolima region by climate class (a) and altitude ranges (b)

2. **Filling in of missing values**

At the beginning, there were between 10% and 50% of missing data according to the studied variables (Appendix F). To fill in the missing climate data, it is common to use daily satellite climate data or statistical methods to model the missing data (Jiménez al., 2021). The *NASA-POWER* satellite database has a spatial resolution of 1.0° latitude by 1.0° longitude for the radiation data sets and 1/2° latitude by 5/8° longitude for the meteorological data sets (NASA,

2020) and is frequently used due to near real-time data availability and its frequent updating and to calculate the reference evapotransporitation of FAO Penman Monteit (Ndiaye & al., 2020 ; Jiménez & al., 2021). Moreover, Luna & al. (2021) showed that the NASA-POWER data provides values with a better accuracy for solar radiation and air temperature than others satellite climatic database, although some estimations with *NASA-POWER* could be worse because of the spatial resolution which provides average values over an area where variation in topography can cause greater climate variability (Jiménez & al., 2021 ; Luna & al., 2021). Hence, daily maximal and minimal temperature values taken at 2 meters of height , daily mean values of wind velocity and of relative humidity taken at 2 meters high, and global irradiance were taken from the *NASA-POWER* database in order to estimate the reference evapotranspiration (Eq. 4). Others satellites data exist for daily precipitations with better spatial resolution could be compared to find data better estimated as precipitation varies strongly in space (Allen & al., 1998), the one with a compromise of the best temporal resolution and the best spatial resolution available in Colombia is "UCSB CHIRPS" with daily values and a possible spatial resolution of $0.05^{\circ} \times 0.05^{\circ}$ latitude longitude (IRI, 2022) and daily total precipitation.

MAE (Eq. 10) and MBE (Eq. 11) were calculated between each station and each satellite database to see which database was most interesting and how reliable these data are (Appendix C). Although the data are usable for the semi-arid region, they are certainly not usable for the semi-humid region, mainly for temperatures and solar radiation respectively under-rated and over-rated by observing the MBE. This could lead to biased simulations. A way must be found to obtain estimates that are more faithful to reality. This is due to the fact that the warm semi-wet climatic zone presents a greater topographic variability over a smaller area than the dry zone, creating a climatic variability not taken into account by average climatic satellite data over the same area (Jiménez & al., 2021).

The table in appendix D shows that most of the satellite and observed variables are significantly correlated by Pearson correlation. A combination with RStudio machine learning-packages to replace missing values were tried to improve the results. Dixneuf (2019) and Alsaber & al. (2021) showed that among these different packages, missForest and MICE combined with random forest presents the best RMSE and MAE performance index on the treatment of environmental multivariable dataset with missing values until 40% missing values. To use that, the dataset must be missing completely at random (MCAR), which means that what causes the missing data is not related to the data itself. The technique missForest was used since it's generally used for this kind of problem (Bender al., 2021) and show sufficient and more or less similar or better results than other missing value imputation techniques (Stekhoven & Bühlmann, 2012 ; Dixneuf, 2019 ; Alsaber & al., 2021). For each variable with missing values, MissForest fits a random forest on the observed part and then predicts the missing part. It first imputes all missing data using the mean or the mode. This training and prediction procedure is repeated repeatedly in an iterative loop until a stopping criterion is satisfied or a maximum number of user-specified iterations has been achieved (Stekhoven & Bühlmann, 2012).

The MAE (Eq. 10), the RMSE (Eq. 12) and the MAPE (Eq. 13) were calculated to evaluate the performance, with a dataset with the same amount of missing values created according the variable (Appendix. F) with the satellite data. The missForest combined with the satellite data gave better estimations for all the variables and no outliers by observing MAE and MAPE, and RMSE (Appendix E).

$$MAE = \frac{1}{n}\sum_{i=1}^{n}|P_i - O_i| \tag{10}$$

$$MBE = \frac{1}{n}\sum_{i=1}^{n} P_i - O_i \tag{11}$$

$$RMSE = \sqrt{\frac{\sum_{i=1}^{n}(O_i - P_i)^2}{n}} \tag{12}$$

$$MAPE = \frac{100}{n}\sum_{i=1}^{n}|\frac{P_i - O_i}{P_i}| \tag{13}$$

Where:

O: Observed values
P: Predicted values
n: Total number of days

3.3.3 Soil parameters values

A series of soils was selected to perform the sensitivity analysis. An analysis on QGIS 3.24 was performed to evaluate the different soils present in rice cultivation and dedicated to agriculture by type of climate in the Tolima region (IGAC, 2004). Based on their textural percentages and organic matter content, the hydrodynamic parameters of water content at PWP, FC and Sat and the hydraulic conductivity at saturation K_{sat} were evaluated via Saxton's pedotransfer curves (Saxton et al., 1986). The penetrability and stoniness values were set homogeneously for all soils. The values of CN and capillarity-defining parameters (Cra, Crb) were taken from the reference values assigned to the soil textural classes of the USDA classification (Raes & al., 2018). These values are listed in the appendix 3.

3.3.4 Irrigation schedule

A border irrigation of 50 mm was applied every five days to simulate non-optimised gravity irrigation as values representative of what is applied (FEDEARROZ, 2017).

4 Results

4.1 Aquacrop simulations for F67 at Nataïma

The performance indices *RMSE* (Eq. 12), *NSE* (Eq. 14) and Pearson's correlation coefficient were used to assess the effectiveness of the canopy cover and soil water content modelling. The NSE is used to assess how well the model accounts for the variability of observed values. If it is equal to 1, it corresponds to a perfect match of modelled to the observed data, if $NSE = 0$, it indicates that the model predictions are as accurate as the mean of the observed data, and if it's negative, it means that the observed mean is better predictor than the model. The RMSE allows to know the deviation of the modelled values from the observed values and to have an idea of how much the values may be outliers. The Pearson coefficient allows to evaluate to what extent the modelled and observed values evolve jointly in time. Moriasi et al. (2007) and Raes et al. (2018) provide reference values of these indices to judge the quality of the modelling done in the hydrology and Aquacrop study areas respectively.

$$NSE = 1 - \frac{\sum_{i=1}^{n}(Q_i^{obs} - Q_i^{sim})^2}{\sum_{i=1}^{n}(Q_i^{obs} - \overline{Q}^{obs})^2} \tag{14}$$

4.1.1 Dry yield

The simulated dry yields (Table 5) show an approximation of the observed data with a global *MBE* (Eq. 11) of 0.621 t/ha, 0.038 t/ha for cycle 1 and 1.204 t/ha for cycle 2. This leads to the conclusion that, overall, the model overestimates the observed values. The hypothesis of respecting the growth orders between the CONTROL treatment and the other two is respected. On the other hand, it is the opposite for the second cycle, the hypothesis of respect of the order of growth of the simulated dry yields between the MIRI-AWD treatment and the two other treatments is not validated, on the contrary, the simulation even shows lower yields than the two other treatments whereas the second crop cycle showed a higher average dry yield for MIRI-AWD (Table 5).

	Obs. yield (t/ha)	Mod. yield (t/ha)	Water depth (mm)	Water Productivity (kg/m^3)
Treatment	Cycle 1			
MIRI	8.467 ±0.909	8.657	788	1.003
MIRI-AWD	8.453 ±1.520	8.536	850	0.932
Control	8.905 ±0.953	8.747	1332	0.641
	Cycle 2			
MIRI	6.648 ±1.053	8.253	639	0.951
MIRI-AWD	7.104 ±1.000	7.656	604	1.070
Control	6.527 ±1.215	7.982	782	0.776

Table 5: Comparison of observed and modelled yields, water depth used (from irrigation and actual rainfall) and water productivity for both cycle

The table also contains the water productivity and the quantities of water applied per cycle. Water productivity can be defined in several different ways, in this case it is the amount of dry yield

produced per volume of water applied in irrigation and by effective rainfall, i.e. rainwater used by the plant and not lost through runoff or deep percolation. The FAO method was used to evaluate it by considering the total monthly rainfall over the whole cycle (Eq. 15).

$$\begin{aligned} P_{Eff} &= 0,6 * P - 10/3 \; if \; P_{month} <= 70/3mm \\ P_{Eff} &= 0,8 * P - 24/3 \; if \; P_{month} > 70/3mm \end{aligned} \tag{15}$$

4.1.2 Canopy cover

The comparison between the evolution over time, for the two cropping cycles, between some observed data such as NDVI (Fig. 5), CC (Fig. 4) and LAI (Fig. 6), and simulated data such as percent canopy cover, shows similar orders of growth for NDVI, CC and LAI, and opposite to the order of growth of simulated water stresses (Appendix Fig. G) for the whole first cycle and the second cycle up to about 70 DAS (Fig. 9b.). The performance indices are shown in table 9. Overall, the simulations are highly correlated with the observations, except for the MIRI-AWD and CONTROL treatments in cycle 2, which also show more outliers than the other treatments. Indeed, these two treatments show an early senescence observed shortly after 70 DAS, whereas the simulations show a recovery of the previously disadvantaged canopy cover. The NSE for the MIRI treatment in Cycle 1 is poor, demonstrating that the difference between the Aquacrop modelled and field observed values is greater than the difference between the observed values and the mean, and that all the variability in the observed values would not be taken into account by the model.

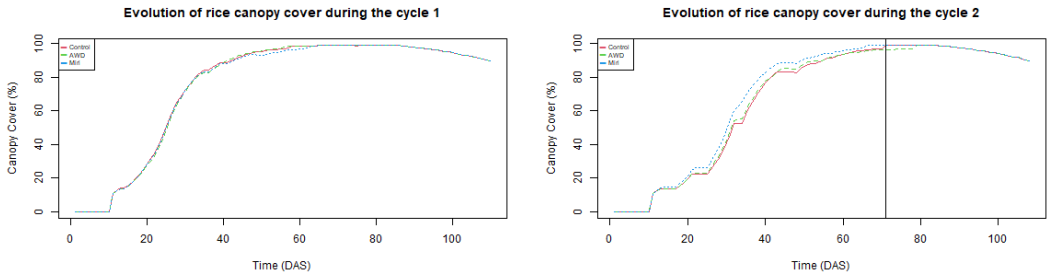

(a) Cycle 1

(b) Cycle 2

Figure 9: Canopy cover modeled for each cycle and treatment

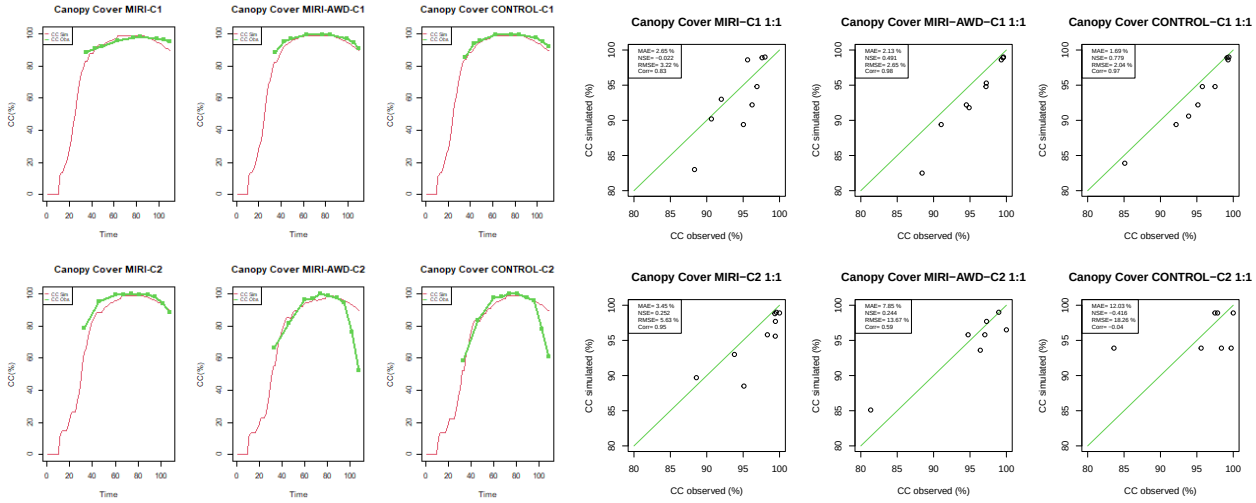

(a) Comparison between observed and simulated canopy cover values

(b) Canopy cover 1:1

Figure 10: Canopy cover modeled for each cycle and treatment

	MIRI	MIRI-AWD	CONTROL
Performance Indice	**Cycle 1**		
NSE	-0,02 Poor	0,49 Moderate good	0,78 Good
Pearson Correlation	0,83 Good	0,98 Very good	0,97 Very good
MAE (%)	2,65	2,13	1,69
RMSE (%)	3,22	2,65	2,04
	Cycle 2		
NSE	0,25 Moderate poor	0,24 Moderate poor	-0,42 Poor
Pearson Correlation	0,95 Very good	0,59 Moderate poor	-0,04 Very poor
MAE (%)	3,45	7,85	12,03
RMSE (%)	5,63	13,67	18,26

Table 6: Performance indices of canopy cover simulations of Aquacrop

4.1.3 Soil water content

The simulated average water contents over a depth of 20 cm were extracted from the output data after deifying the soil water content in a compartment between 0 and 20 cm on Aquacrop. The evolution of the modelled and observed water contents for each cycle and each treatment are shown in Figure 1 and the performance indices in Table 2. Overall the simulations are rather poor. For cycle 1, the values are largely underestimated, more so than for cycle 2. The Pearson coefficient shows that the simulated water content for both cycles does not evolve in the same way over time as the measured data. However, the measurements and the modelled values seem to be in better agreement for cycle 2

	MIRI	MIRI-AWD	CONTROL
Performance Indice	**Cycle 1**		
Pearson correlation	0.40	0.27	0.28
		Poor	
NSE	-10.01	-8.50	-9.96
		Poor	
RMSE (%Vol)	18.35	14.27	17.82
	Cycle 2		
Pearson correlation	0.41	0.23	0.35
		Poor	
NSE	-3.73	-3.55	-0.95
		Poor	
RMSE (%Vol)	5.80	6.90	5.41

Table 7: Performance indices of soil water content simulations of Aquacrop

than for cycle 1, showing a better *RMSE*, as well as a *NSE* closer to zero, demonstrating that it would be more reliable in general to refer to the observed mean value than to the simulations.

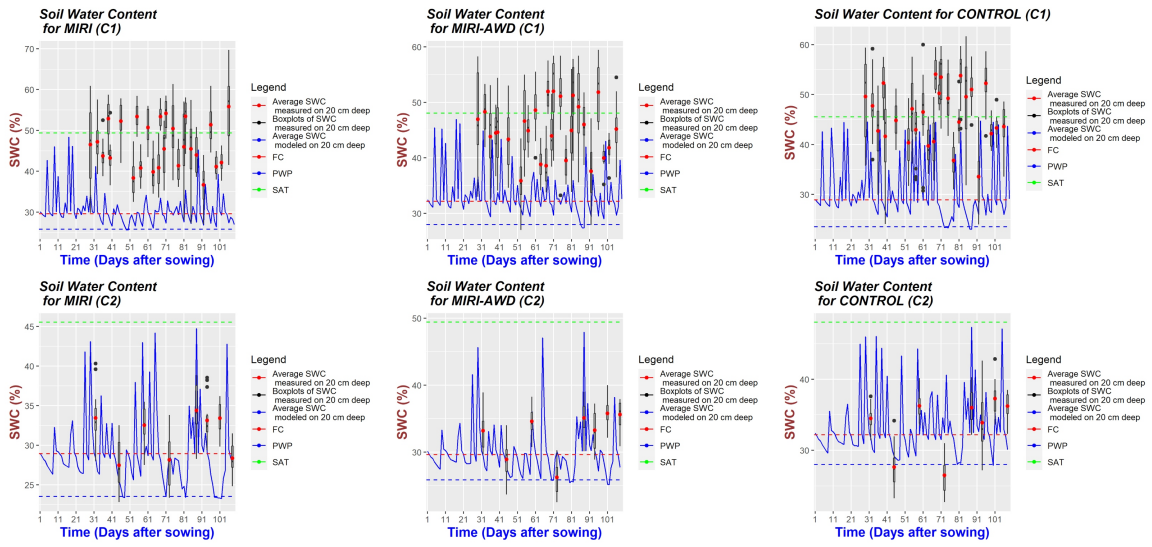

Figure 11: Evolution of simulated and observed soil water content for each treatment and cycle

4.2 Sensitivity analysis

The figures show the graphs representing for each output variable, the absolute mean $\mu*$ of all the elementary effects of each input as a function of the standard deviation $\mu*$ of the elementary effects means for all the trajectories and days of the simulations. The horizontal bars parallel to the x-axis around the points show the standard deviation of the absolute means of the elementary effects due to variability across different soils, climates and years, while the vertical bars represent the standard deviations of the standard deviations also describing environmental and temporal variabilities. The figure shows a decreasing ranking of the absolute means of the elementary effects by parameter.

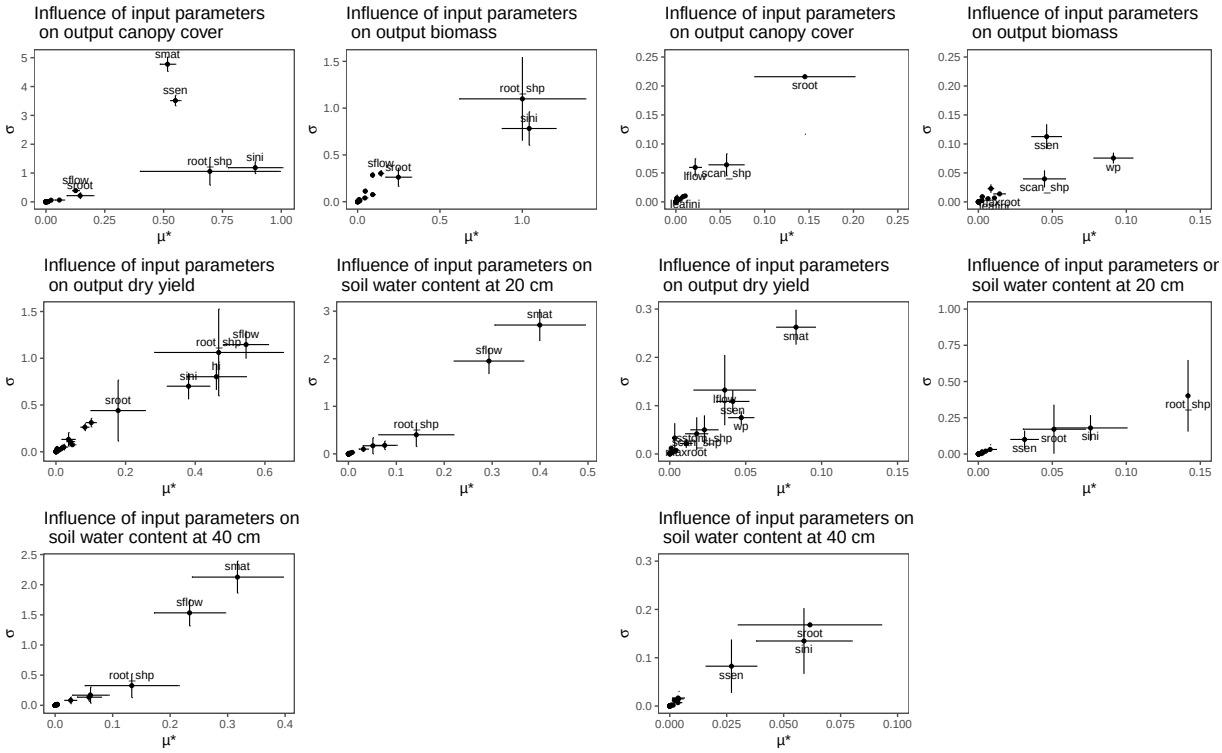

(a) Global screening

(b) Zoom on lower values

Figure 12: Inspection of the elementary effect statistics on the σ versus $\mu*$ plane

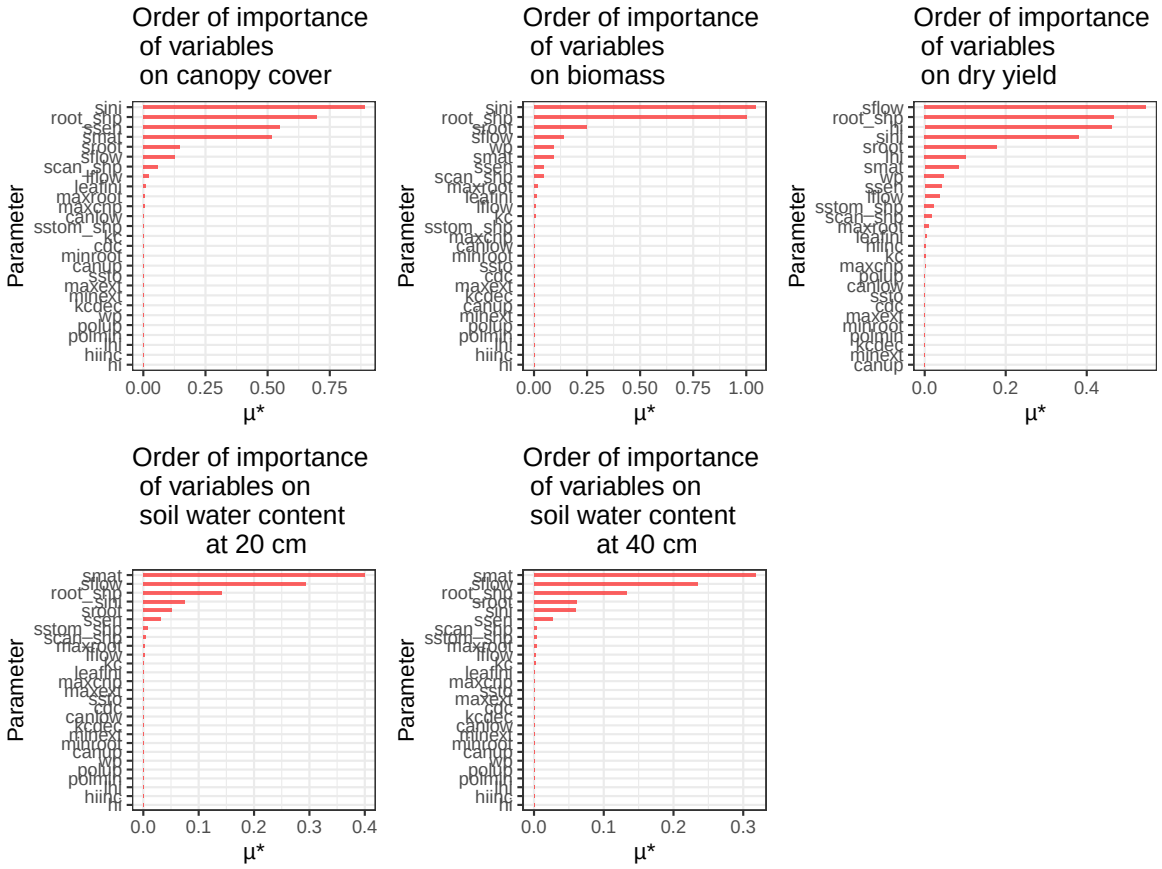

Figure 13: Ranking of absolute means of elementary effects by input parameter for each output variable

Morris (1991) provides different indications to classify and evaluate the importance of input parameters. The notions of influential and non-influential parameters are based on the relative locations of those statistics in the plane and the analysis is generally done qualitatively. A relatively high value of $\mu*$ combined with a relatively low value of σ indicates that it is a parameter with a linear effect on the output variable, as the elementary effects have little variation between them and a relatively large absolute average of the variation in output caused by the variation in input. Conversely, a relatively high value of σ and a relatively low value of $\mu*$ demonstrate a high variability in the output variation caused by a parameter variation, showing a non-linear effect or an interaction with other parameters. If the standard deviation and mean values are more or less equivalent, the relationship can be considered monotonic.

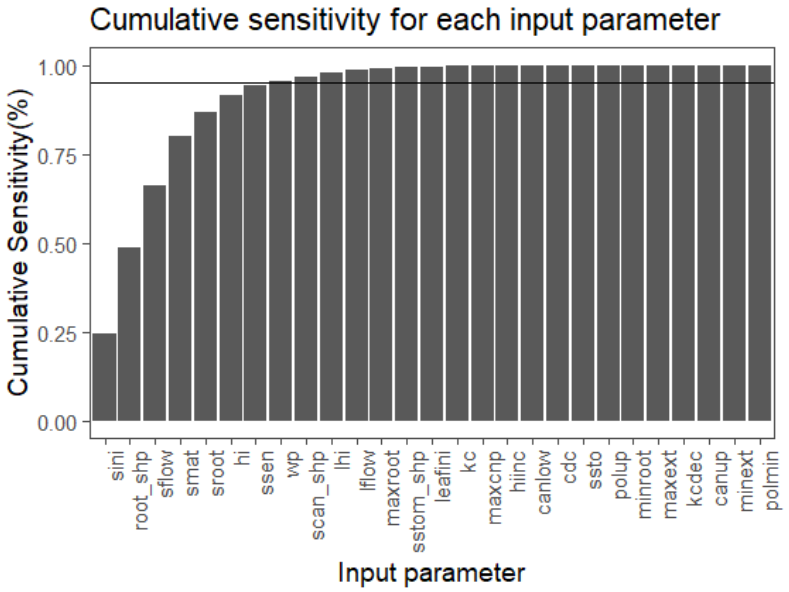

Figure 14: Cumulative sensitivity on all the studied output

5 Discussions and proposals

5.1 Discussions about dry yield simulations and canopy cover

As explained earlier, the irrigation system was worked on during the first 30 days, leaving the crop to be fed only with rainwater. The crops were therefore under greater stress than in Cycle 1. The figure shows the modelled evolution of the canopy covers, which differs significantly for the MIRI, which shows higher growth from 10 DAS. Aquacrop considers different water stresses impacting the development of the crop in different ways and triggered when depletion percentages of the TAW are exceeded. The triggering thresholds for these stresses are conservative parameters and are listed in the appendix. The three consequences of water stresses ranked in order of growth according to the percentage of TAW depletion are: impact on canopy development, stomatal closure and early senescence. At about 15 DAS, Aquacrop considered the impact of early senescence and stomatal closure to be less important for the MIRI treatment than for the other two treatments and critical for biomass development in the remainder of the cycle, since this treatment has a relatively slightly lower and wider TAW than the other two treatments (Fig.). However, although no field observations were made before 30 DAS and do not validate this hypothesis at that time, data taken from 30 days onwards show higher LAI, NDVI and CC values for the MIRI treatment over the whole crop cycle (Fig. 5 b. ; 6b. & 4b.).

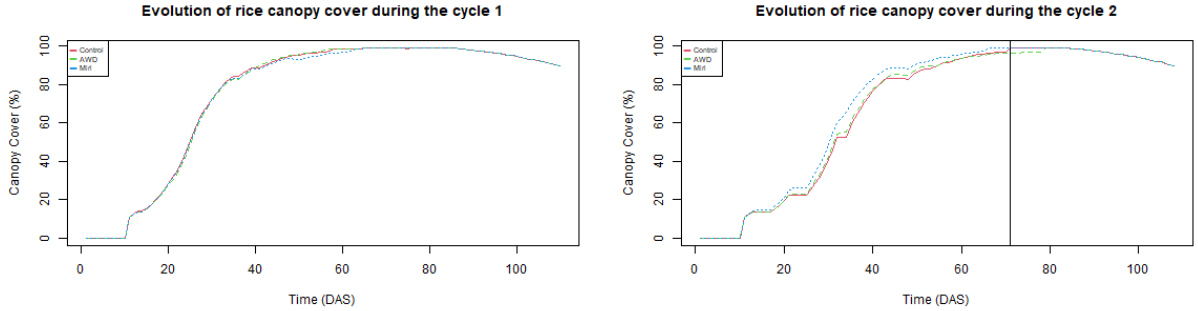

(a) Cycle 1

(b) Cycle 2

Figure 15: Inspection of the elementary effect statistics on the σ versus $\mu*$ plane

However, this still does not explain why the MIRI-AWD shows a higher dry yield that cannot be modelled despite this relatively lower canopy growth trend and similar to the MIRI and CONTROL respectively (Fig. 4b.; 9). There are many possible explanations for this phenomenon, and Aquacrop considers a number of them. Firstly, the stresses of lack of pollination and sterility, and reduced transpiration due to cold, respectively impact on the development of percentage dry yield and biomass as a function of the relative exceedance of maximum and minimum temperature threshold values listed in the appendix 8. However, these values were never exceeded during the hypothetical flowering period and even over the whole cycle (Fig. 17). As explained under 3.2.3, stresses related to anoxia or soil salinity are also irrelevant.

Rice becomes increasingly sensitive to drought as the vegetative phase advances and during the reproductive and grain-filling phase (Wopereis et al., 1996), which can decrease dry yield (O'Toole, 1982). On Aquacrop, rice is initially calibrated so that the Harvest Index is increased in case of canopy development stress only during the grain filling phase and decreased in case of stomatal closure during this same phase (Steduto & al., 2012). This probably explains the higher harvest index in cycle 2, above 60%, in view of the still unexplained decrease in leaf biomass observed with a relatively higher grain mass than in cycle 1 (Fig. 4b.; 5b.). HI can also be increased during the vegetative phase due to leaf development stress, but this parameter is initially set to zero for rice and is a conservative parameter. Simulations run by increasing the magnitude of the HI increase parameters do increase the simulated yield, but for all three treatments, without yet explaining the decrease in canopy for the MIRI-AWD and CONTROL treatments and the higher dry yield of MIRI-AWD. We should therefore be more interested in factors that may have acted heterogeneously on the three treatments, deviating the simulations from the observations.

Two hypotheses were retained, that of the arrival of the disease due to the arrival of a bacterium or a fungus and that of the heterogeneous application of fertilisers. Other factors that may occur heterogeneously are debatable, such as simple human error in data collection or the infestation of a crop pest or weed. That said, although Aquacrop is able to account for the impact of weed presence in its simulations, herbicides, as well as insecticides, were applied evenly across all three treatments and no weeds were observed during field visits.

5.1.1 Disease hypothesis

The figures show that around 81 DAS, the AWD and control treatments have CC values that differ from the simulated values, and that afterwards the canopy coverages decrease drastically compared to that of the MIRI and the simulations around 89 DAS. These discrepancies need to be investigated in

more detail. Figure 17 shows that from 80 DAS onwards the most intense precipitation periods of the cycle take place. In addition, these two treatments were irrigated a few days after these events and the MIRI only after two weeks. Analysis of the NDVI over the whole plot (Fig. 16) after the end of these events shows the development of a concentric spot on the three plots describing a drop in NDVI values compared to the rest of the crop areas, and mainly on the MIRI-AWD and CONTROL plots. This spot persists until 122 DAS, just before harvest, and is visible in both UAV and Sentinel-2 satellite images (Fig.). Finally, it occurs after the CC has been maximised. One hypothesis is that this could be the result of the spread of a bacterium or fungus. Indeed, the occurrence of this type of event in a concentric way occurs preferentially when the canopy is maximum, favouring a horizontal spread on the crop (Kozaka, 1961). During contamination, the chlorophyll content decreases, causing a higher reflectance in the red and blue visible wavelength spectra and a decrease in reflectance in the NIR, and thus a decrease in detectable NDVI (Zhang et al., 2017; Gogoi et al., 2018).

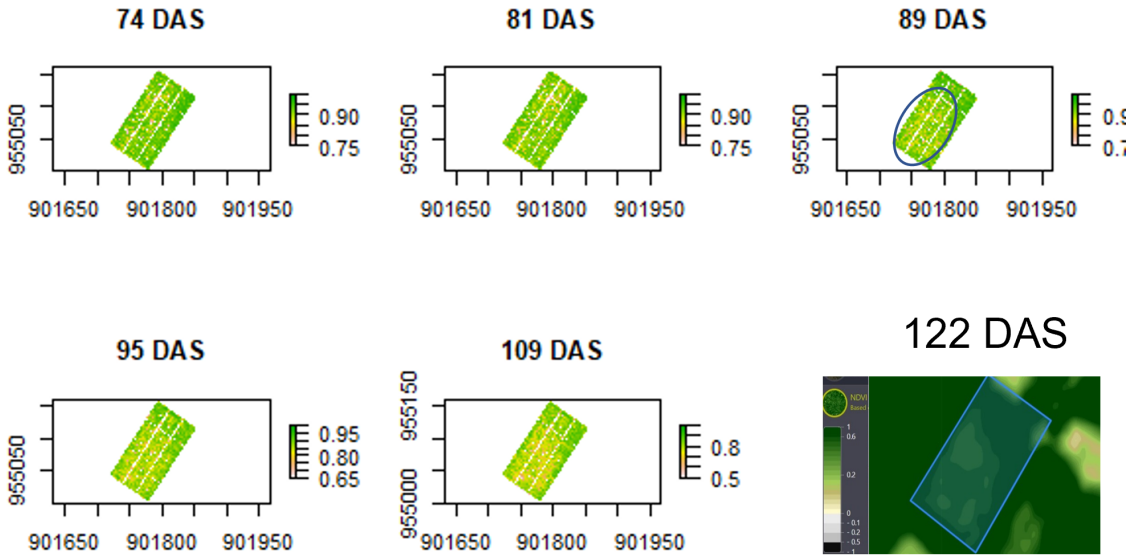

Figure 16: Evolution of the global NDVI measured with UAV and Sentinel-2 images on all three plots. Left: MIRI-AWD, Center: CONTROL, Right: MIRI

The F67 variety is known to be resistant to *Pyricularia grisae* Sacc. and white leaf disease (Ocampo Henao, 2019), and *Burkholderia glumae* L. (Echeverri & al., 2019). However, it is not known to be especially resistant to other leaf-spotting pests common in rice crops in these regions such as *Rhizoctonia solani* Kühn (Pod blight), *Bipolaris orizae* (Breda de Haan) Shoemaker (Helmintosporiosis), *Sarocladium oryzae* (Sawada) W. Gams D. Hawksw (pod rot), *Rhynchosporium oryzae* Hashioka Yokogi ("Escalado") and *Gaeumannomyces graminis* (Sacc.) Arx & D.L.Olivier ("Mancha Café") (Tacha, 2015).

However, these diseases are known to have an impact on yield. In this case, the treatment with the highest leaf senescence was MIRI-AWD, which gave a possibly higher dry yield than the other two treatments. In addition, the fungicide treatment 'Nativo' was applied 81 DAS as a preventive measure, i.e. a few days before the appearance of the concentric spots on the drone images and at the beginning of the heavy rainfall. However, it was applied at a rate of 0.5 L/ha, while the product, however combined with the additive "Agrotin", is effective against almost all the above mentioned diseases but should be applied at a recommended rate of 0.8 to 1 L/Ha (BAYER S.A., 2021).

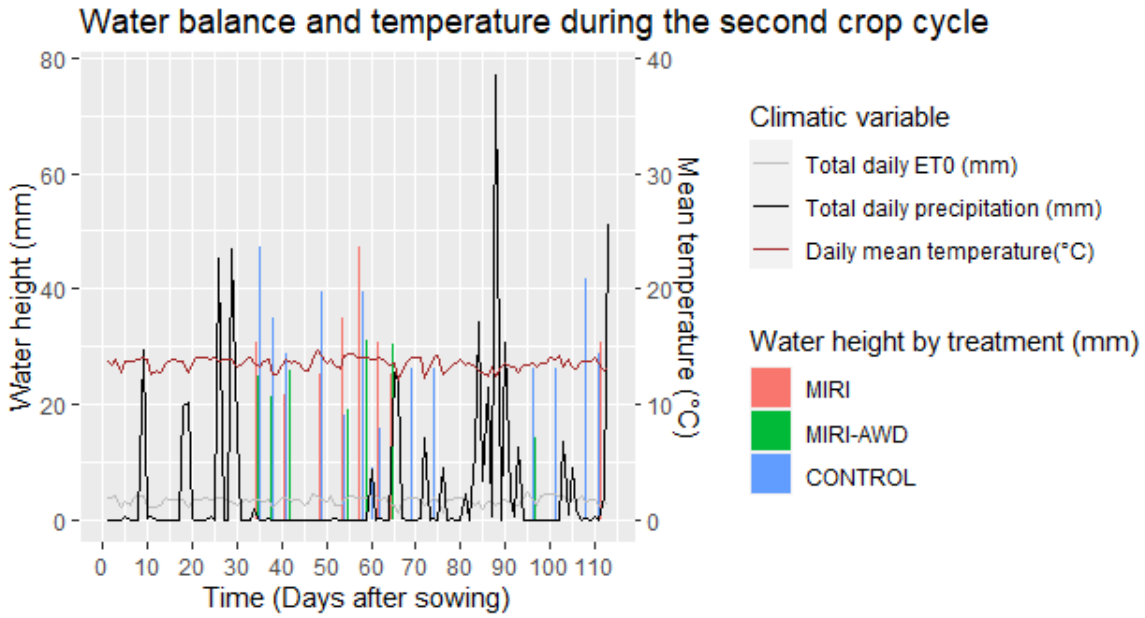

Figure 17: Water balance and temperature during the second crop cycle

5.1.2 Fertility hypothesis

However, as mentioned above, these concentric patches of decay could also simply correspond to early leaf senescence due to fertility. Indeed, fertility stress was not calibrated in Aquacrop. The leaf blades are able to mobilise a lot of nitrogen to supply it to the panicles, causing an acceleration of senescence and a decrease in photosynthetic activity (Fageria, 2007). Therefore, slower senescence is preferable, to allow photosynthesis to provide more grain filling until maturity (Jennins et al., 1979). The theory of a higher N dose applied to MIRI-AWD and CONTROL in cycle 2 can be considered in that they clearly demonstrate early senescence, although only one last fertiliser dose was applied similarly on all three plots at around 81 DAS, and the divergence in canopy cover behaviour in the second cycle from the simulations was detected from the 89 DAS measurement.

However, the MIRI-AWD treatment showed a significantly higher number of panicles than the other two treatments, which may explain the higher dry yield. The optimal number of panicles developed as a function of nitrogen application is mainly determined during the vegetative phase (Fageria Baligar, 1999). Nitrogen application during the reproductive phase, during booting (panicle development) and flowering, does not cause an increase in panicle number (Fageria, 2007). These facts could also suggest that the MIRI-AWD treatment was exposed to a higher N application rate. Unfortunately, data on the nitrogen concentration in the soil could not be obtained.

5.2 Discussions about soil moisture simulations

The simulated data for cycle 1 clearly underestimates what was observed. There is therefore more water stress simulated by Aquacrop. Although Aquacrop gives interesting crop development results compared to the observed data, these values should be reviewed, because if Aquacrop had not simulated these stresses, the biomass values would have been even higher, while the model already overestimates the simulations. One hypothesis could be that the modelled saturation conductivity was overestimated and could be re-evaluated with more samples. However, the measurements already made seem to vary significantly spatially. Indeed, spatial variation in paddy soils due to sediment deposition and changes in soil fertility and organic carbon content that are spatially heterogeneous over the course of a cycle are known (Schmitter al, 2010). This has the effect of modifying the hydrodynamic parameters of the

soil, as explained in point **??**. Furthermore, Aimrun et al (2004) demonstrated coefficients of variation of hydraulic conductivity at saturation of about 140% in paddy soils. So although studies have shown that soil water content can be simulated in good performance ranges (Belkhiri Semiani, 2019; Porras-Jorge al., 2020), this seems to be compromised in the present study case. Saturation conductivity measurements could be measured on a larger scale to get a better overview. Alternatively, other pedotransfer curves could also be studied and evaluated later, such as *Rosetta* (Schaap & al., 2001) or *Hypres* (Wösten & al., 1999) operating by ANN and linear regression respectively, and calibrated on American and European soil databases.

Another interesting point is that the water content measured during the cycle sometimes exceeds the saturation values evaluated for the soils. The TDR 350 instrument had been used, so a recalibration of the instrument may be necessary, although the ranges of values appear to be less aberrant for cycle 2 (Fig. 11).

5.3 Discussions about sensitivity analysis

The absolute means of the elementary effects were combined across all output variables to investigate the cumulative sensitivity of the input parameters (Fig. 14). The eight input parameters *sini*, *rootshp*, *sflow*, *smat*, *sroot*, *ssen* and *hi* account for 95% of the total sensitivity. These parameters should be evaluated first in the framework of simulations launched on Aquacrop in the Tolima region. Overall, the duration of the phenological stages is important in the impact on all output variables (Fig. 14). The parameters *smat* and *ssen* appear to have a non-linear or interfering effect with respect to canopy development. The parameters *sflow* and *smat* have the same effect on soil water content. The parameters *rootshp* and *sroot* seem to show a great variability according to the environment due to climatic variability and whose impact on root development is taken into account by the climate and hydrodynamic parameters of the soils during stress. Moreover, this is probably the same cause of variability in the elementary effects of *sflow* and *smat*. *sini* seems to show a monotonic influence on the outputs on CC, biomass and dry yield. The parameters *hi*, *lhi* and *wp* obviously show a monotonic effect on the dry yield. The parameter *rootshp*, describing the concavity of the root depth development curve over time, also appears to be a parameter whose variation has relatively more impact on the variation of outputs, either with linear or monotonic relationships, and with a large variation of elementary effects across environments.

It would be interesting to develop the treatment of these values further. Firstly, to carry out analyses according to regions and soil types in order to study the change in the order of importance of the input variables within them. Coudron et al (2021) provided work analysing the collinearity between elemental effects across different soils and years to establish optimised data recovery methodologies with respect to the environment and the intervals of days of measurement over the cycle in order to calibrate Aquacrop as easily as possible.

6 Conclusion

In conclusion, the simulation results show good performance for the first cycle, which was mainly used for calibration. However, for the second cycle, the simulations are less good except for the MIRI treatment. Aquacrop evaluated the dry yield of the CONTROL treatment as superior to the other treatments, fulfilling the hypothesis of a potential small statistical difference. However, the simulated dry yields for the second treatment differed more than for Cycle 1. Indeed, the simulations do not allow to simulate the higher dry yield of the MIRI-AWD treatment. This can be explained by a significantly higher number of panicles which could have been influenced by the fertilisation before flowering. Concerning the development of the canopy cover, the model provided very good results for cycle 1, but much worse results for the second validation cycle. A decrease explained by no stress taken into account by the model with the environmental data considered occurs on two treatments. The hypotheses of excessive fertilisation, the appearance of a fungal or bacterial parasite, or human error during the taking of measurements and processing of data are retained.

The sensitivity analysis shows which variations in crop parameters most influence certain output variables, as well as the variations in the influence of these parameters across the environment encountered in rice crops in the Tolima region. It was found that the time to reach maturation, flowering, emergence, maximum root development and senescence, as well as the shape parameter of root development over time and the cropping index had the greatest impact. Further analysis could be considered.

A Appendix

Description	Type[1]	Method[2]	Value	Source
Canopy size of the average seedling at 90% emergence, or canopy size of the transplanted seedling (cm^2)	Co Ma	E	2,9	
Number of plants per m^2	Ma	M		
from				
• 1000 grain mass (mg)	Cu	M L	28	Tirado and Castilla Lozano, 2019 Burgos Bedoya, 2021 Heros and al., 2022
• Sowing density (kg/ha)	Ma	M	170 (C1) 150 (C2)	
Time from sowing to emergence (days or GD days) or recovery time (for transplanted seedlings)	Ma	L	10	Herrera Vidal, 2020 Burgos Bedoya, 2021 Gomezcasseres Argumedo, 2021
Maximum canopy cover (fraction soil cover)	Cu	M	99	
Time from sowing to maturity, i.e length of crop cycle (days or GD days)	Cu	M	110	Herrera Vidal, 2020 Burgos Bedoya, 2021
Time from sowing to flowering or to the start of yield formation (days or GD days)	Cu	M L	75	Herrera Vidal, 2020 Burgos Bedoya, 2021 Gomezcasseres Argumedo, 2021
Time from sowing to start senescence (days)	Cu	M	85	
Length of the flowering stage (days or GD days)	Cu	L	13	Fernandez, 2013 Melo Solarte, 2019
Minimum effective rooting depth (m)	Ma	L	0,15	Allen and al., 1998 Granados, 2021
Maximum effective rooting depth (m)	Ma	L	0,30	Tirado and Castilla Lozano, 2017 SATREPS, 2019 Granados, 2021
Time to reach maximal root depth (days)	Ma	L	70	Fageria, 2007
Shape factor describing root zone expansion	Co	C	25	

Description	Type[1]	Method[2]	Value	Source
Crop performance under elevated atmospheric CO2 concentration (%)	Ma Cu	C	20	
Reference harvest index (%)	Cu	M L	47	Heros and al., 2022
Excess of potential fruits (%)	Co	C	0	
Possible increase (%) of HI due to water stress before flowering	Co	C	0	
Coefficient describing positive impact of restricted vegetative growth during yield formation on HI	Co	C	4.0	
Coefficient describing negative impact of stomatal closure during yield formation on HI	Co	C	5.0	
Allowable maximum increase (%) of specified HI	Co	C	15	
Vol% at anaerobiotic point (with reference to saturation)	Cu Env	L	0	Miro Ismail, 2013
Canopy growth coefficient (fraction per day or per growing degree day)	Cu	M	12	
from • Time for sowing to maximal canopy cover (days or GD days)	Cu	M	50	
Canopy decline coefficient (fraction per day)	Cu	C	4,2	
Crop coefficient when canopy is complete but prior to senescence	Co	C	1,10	
Decline of crop coefficient (% of CCx per day) as a result of ageing, nitrogen deficiency, etc.	Co	C	0,150	
Maximum root water extraction (m3/m${-3}$/day) in top quarter of root zone	Ma	C	0,048	
Maximum root water extraction (m3/m${-3}$/day) in bottom quarter of root zone	Ma	C	0,012	

Description	Type[1]	Method[2]	Value	Source
Effect of canopy cover in reducing soil evaporation in late season stage (% reduction in soil evaporation)	Co	C	50	
Water productivity normalized for ETo and CO2(gram/m2)	Co	C	19	
Reduction coefficient describing the effect of t he products synthesized during yield formation on the normalized water productivity	Co	C	0	
Soil water depletion threshold for canopy expansion - Upper threshold (fraction of RAW)	Co	C	0,00	
Soil water depletion threshold for canopy expansion - Lower threshold	Co	C	0,40	
Shape factor for Water stress coefficient for canopy expansion	Co	C	3.0	
Soil water depletion threshold for stomatal control –Upper threshold	Co	C	0,50	
Shape factor for Water stress coefficient for stomatal control	Co	C	3.0	
Soil water depletion threshold for canopy senescence – Upper threshold	Co	C	0,55	
Shape factor for Water stress coefficient for canopy senescence	Co	C	3.0	
Soil water depletion threshold for failure of pollination – Upper threshold	Co	C	0,75	
Minimum air temperature below which pollination starts to fail (cold stress) (°C)	Co	C	0	
Maximum air temperature above which pollination starts to fail (heat stress) (°C)	Co	C	35	
Soil fertility stress Shape factor for the stress coefficient for canopy expansion	Ma	NU	-	
Soil fertility stress Shape factor for the stress coefficient for Maximum Canopy Cover	Ma	NU	-	

Description	Type[1]	Method[2]	Value	Source
Soil fertility stress Shape factor for the stress coefficient for Crop Water Productivity	Ma	NU	-	
Soil fertility stress Shape factor for the response of Decline of Canopy Cover to stress	Ma	NU	-	
Electrical Conductivity of soil saturation extract at which crop starts to be affected by soil salinity (dS/m)	Ma	C	3	
Electrical Conductivity of soil saturation extract at which crop can no longer grow (dS/m)	Ma	C	11	

Table 8: All crop parameters used for F67 in Aquacrop, 1. **Co** : Conservative generally applicable ,**Ma/Env** : Dependent on environment and/or management, **Cu** : Cultivar specific, **E**: Estimated, 2. **C**: Calibrated **M**: Measured **L**: Litterature **NU**: Non used

B Appendix

Name	Horizon	Thick-ness (m)	Sat (%)	FC (%)	PWP (%)	Ksat (mm/day)	CRa	CRb	CN	Relative area (%)
BT66	Ap	0,15	46,00	38,40	25,00	26,88	-0,61	0,59	77	5,2
	Bw	0,55	52,10	46,50	34,10	10,56	-0,61	0,59	77	
14R	Ap	0,15	45,60	37,20	22,70	37,44	-0,52	1,62	72	2,4
	Bw	0,35	45,10	36,80	22,70	36,96	-0,57	-0,86	72	
5G	Ap	0,15	49,30	40,50	27,70	40,32	-0,61	0,59	77	5,2
	AB	0,18	51,40	44,60	31,70	18,72	-0,61	0,59	77	
	Bw	0,37	53,50	45,50	32,80	30,00	-0,61	0,59	77	
PH1	A	0,40	43,40	23,60	12,30	436,08	-0,32	0,22	46	15
	C	0,10	42,20	33,20	21,50	43,92	-0,58	-0,51	72	
G3-S13	Ap	0,40	42,70	20,70	11,70	620,40	-0,32	0,22	46	11
	Bw	0,10	42,70	20,70	11,70	453,36	-0,32	0,22	46	
PT30	A	0,40	44,10	20,20	10,90	792,00	-0,32	0,22	46	13
	AC	0,10	44,10	20,20	10,90	582,24	-0,32	0,22	46	
PT29	A	0,15	38,40	14,20	5,80	1226,88	-0,32	0,22	46	7,8
	C	0,20	41,40	5,20	0,40	4454,64	-0,34	0,44	46	
PA7	Ap	0,15	39,20	24,60	14,40	190,32	-0,58	-0,51	72	5,2
	A	0,07	38,40	14,90	7,00	808,08	-0,32	0,22	46	
	Bw	0,26	39,00	23,20	12,00	67,92	-0,45	0,84	61	
BT79	Ap	0,12	38,80	22,50	10,90	282,72	-0,45	0,84	61	14
	A	0,28	40,60	28,70	16,80	104,88	-0,57	-0,86	72	
	Bw	0,20	41,50	30,80	18,00	78,24	-0,57	-0,86	72	
P-1	A	0,40	38,80	12,40	5,60	1115,76	-0,32	0,22	46	10,5
	Bw	0,10	39,00	11,60	5,60	1220,16	-0,32	0,22	46	
T-21	A	0,40	40,00	26,90	14,50	104,40	-0,45	0,84	61	10,5
	Bw1	0,10	41,00	29,40	15,70	73,44	-0,45	0,84	61	

Table 9: Table of hydrodynamic parameters of the different soils used by Aquacrop for the sensitivity analysis

C Appendix

	Warm semi-humid climate data		Warm semi-arid climate data	
	MAE	MBE	MAE	MBE
Precip ($mm.d^{-1}$) Obs-CHIRPS	4	3	3	2
Precipitation ($mm.d^{-1}$) Obs-NP	5	4	5	2
Max. Temperature (°C) Obs-NP	10,9	-10,9	1,9	-0,6
Min. Temperature (°C) Obs-NP	5,3	-5,2	1,3	-0,6
Solar Radiation ($MJ.m^{-2}.d^{-1}$) Obs-NP	10,106	10,104	2,486	-0,946
Relative Humidity (%) Obs-NP	7	5	8	-7
Wind Velocity ($m.s^{-1}$) Obs-NP	0,38	-0,27	0,47	-0,08

Table 10: MAE and MBE describing the mean errors between measured and satellite modelled climate data

D Appendix

	RH NP	Solar radiation NP	Max temperature NP	Min temperature NP	Wind velocity NP	Pre
RH obs	0,00	0,00	0,00	0,00	0,00	0,0
Precipitation obs	0,00	0,00	0,00	0,00	0,00	0,0
Solar radiation obs	0,00	0,00	0,00	0,00	0,00	0,0
Max temperature obs	0,00	0,00	0,00	0,00	0,00	0,0
Min temperature obs	0,00	0,17	0,00	0,00	0,00	0,0
Wind velocity obs	0,00	0,00	0,00	0,00	0,01	0,0

Table 11: p-values of Pearson correlation test

E Appendix

	MAE	RMSE	MAPE (%)
Relative Humidity (%)	3	4	1,34
Precipitation ($mm.d^{-1}$)	2	3	-
Solar Radiation ($MJ.m^{-2}.d^{-1}$)	3,158	4,199	6,04
Max. Temperature (°C)	1,3	1,7	1,40
Min. Temperature (°C)	0,9	1,1	1,15
Wind Velocity ($m.s^{-1}$)	0,21	0,28	6,80

Table 12: Performance index between modelled and observed values with the MICE-RandomForest method

F Appendix

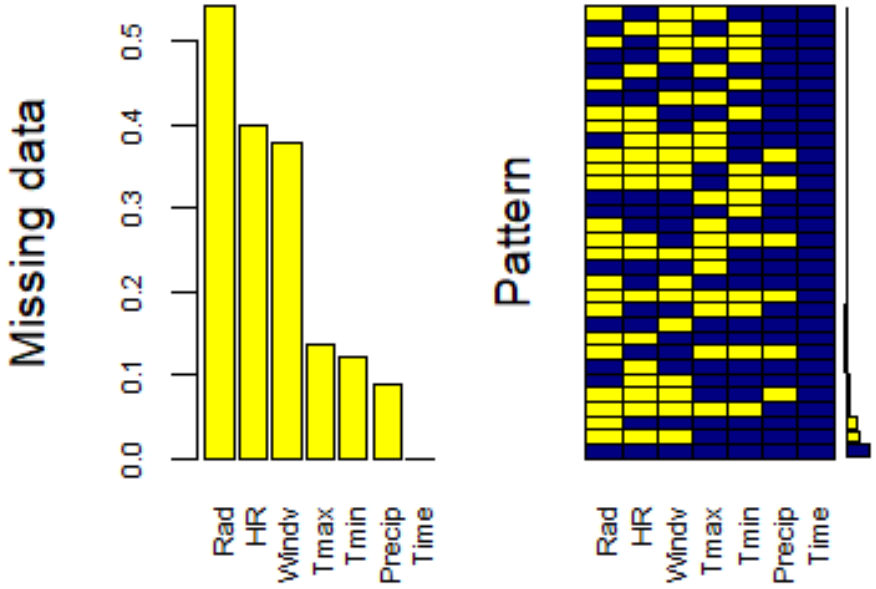

Figure 18: Initial missing values

G Appendix

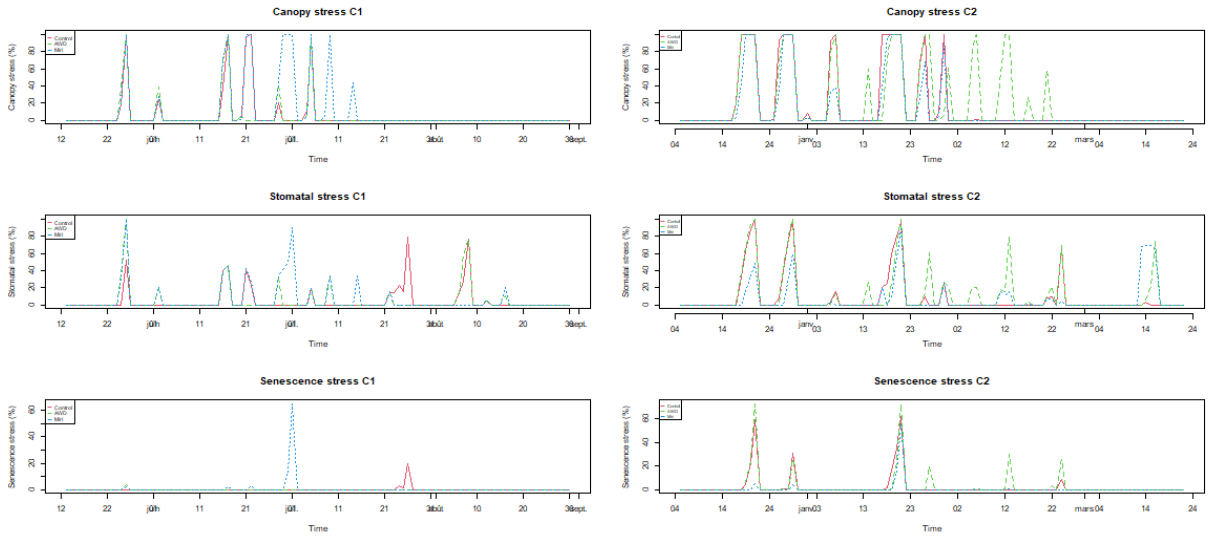

(a) Cycle 1

(b) Cycle 2

Figure 19: Inspection of the elementary effect statistics on the σ versus $\mu*$ plane

7 Bibliography

30-Meter SRTM Elevation Data Downloader [WWW Document], n.d. URL https://dwtkns.com/srtm30m/ (accessed 7.14.22).

Abedinpour, M., Sarangi, A., Rajput, T.B.S., Singh, M., Pathak, H., Ahmad, T., 2012. Performance evaluation of AquaCrop model for maize crop in a semi-arid environment. Agricultural Water Management 110, 55–66. https://doi.org/10.1016/j.agwat.2012.04.001

Ahuja, L.R., Cassel, D.K., Bruce, R.R., Barnes, B.B., 1989. Evaluation of spatial distribution of hydraulic conductivity using effective porosity data. Soil Science 148, 404–411.

Aimrun, W., Amin, M.S.M., Eltaib, S.M., 2004. Effective porosity of paddy soils as an estimation of its saturated hydraulic conductivity. Geoderma 121, 197–203. https://doi.org/10.1016/j.geoderma.2003.11.010

Allen, R.G., Pereira, L.S., Raes, D., Smith, M., 1998. Crop evapotranspiration-Guidelines for computing crop water requirements-FAO Irrigation and drainage paper 56. Fao, Rome 300, D05109.

Allen, R.G., Walter, I.A., Elliott, R., Howell, T.A., Itenfisu, D., Jensen, M.E., 2005. The ASCE standardized reference evapotranspiration equation.

Alsaber, A.R., Pan, J., Al-Hurban, A., 2021. Handling Complex Missing Data Using Random Forest Approach for an Air Quality Monitoring Dataset: A Case Study of Kuwait Environmental Data (2012 to 2018). International Journal of Environmental Research and Public Health 18, 1333. https://doi.org/10.3390/ijerph18031333

Angstrom, A., 1924. Solar and terrestrial radiation. Report to the international commission for solar research on actinometric investigations of solar and atmospheric radiation. Quarterly Journal of the Royal Meteorological Society 50, 121–126. https://doi.org/10.1002/qj.49705021008

Ansoleaga, U.L., 2021. How to Detect, Handle and Visualize Outliers [WWW Document]. Medium. URL https://towardsdatascience.com/how-to-detect-handle-and-visualize-outliers-ad0b74af4af7 (accessed 7.18.22).

Arshad, M., Nisar, S., Gul, I., Nawaz, U., Irum, S., Ahmad, S., Sadat, H., Mian, I.A., Ali, S., Rizwan, M., Alsahli, A.A.,

Alyemeni, M.N., 2021. Multi-element uptake and growth responses of Rice (Oryza sativa L.) to TiO2 nanoparticles applied in different textured soils. Ecotoxicology and Environmental Safety 215, 112149. https://doi.org/10.1016/j.ecoenv.2021.112149

Barrero, O., Ouazaa, S., Jaramillo-Barrios, C.I., Quevedo, M., Chaali, N., Jaramillo, S., Beltran, I., Montenegro, O., 2019. Rice Yield Prediction Using On-Farm Data Sets and Machine Learning, in: International Conference on Smart Information Communication Technologies. Springer, pp. 422–430.

Bayer S.A., 2021. FICHA TÉCNICA NATIVO.

Belkhiri, F.-E., Semiani, M., Heng, L., 2019. CALIBRATION DU MODELE FAO AQUACROP POUR LA CULTURE DU BLE EN CONDITIONS MEDITERRANEENNES 18, 23–44.

Bender, A., Moner-Girona, M., Becker, W., Bódis, K., Szabó, S., Kararach, A.G., Anadon, L.D., 2021. Dataset for multidimensional assessment to incentivise decentralised energy investments in Sub-Saharan Africa. Data in Brief 37, 107265. https://doi.org/10.1016/j.dib.2021.107265

Benitez, M.R., 2020. Todo sobre la Piricularia y las enferdades fúngicas del arro [WWW Document]. URL https://www.agro.basf.es/es/Camposcopio/Secciones/Enfermedades-y-plagas/Todo-sobre-la-Piricularia/ (accessed 8.11.22).

Boote, K.J., Jones, J.W., Pickering, N.B., 1996. Potential Uses and Limitations of Crop Models. Agronomy Journal 88, 704–716. https://doi.org/10.2134/agronj1996.00021962008800050005x

Brun, R., Reichert, P., Künsch, H.R., 2001. Practical identifiability analysis of large environmental simulation models. Water Resources Research 37, 1015–1030. https://doi.org/10.1029/2000WR900350

Burgos Bedoya, C.A., 2021. Evaluación de crecimiento y rendimiento de cuatro variedades y una línea avanzada de arroz (Oryza sativa L.) en el centro experimental la victoria-fedearroz Montería-Córdoba.

Cairns, J.E., Impa, S.M., O'Toole, J.C., Jagadish, S.V.K., Price, A.H., 2011. Influence of the soil physical environment on rice (Oryza sativa L.) response to drought stress and its implications for drought research. Field Crops Research 121, 303–310. https://doi.org/10.1016/j.fcr.2011.01.012

Campbell, G.S., Norman, J.M., 1989. The description and measurement of plant canopy structure, in: Marshall, B., Russell, G., Jarvis, P.G. (Eds.), Plant Canopies: Their Growth, Form and Function, Society for Experimental Biology Seminar Series. Cambridge University Press, Cambridge, pp. 1–20. https://doi.org/10.1017/CBO9780511752308.002

Campolongo, F., Cariboni, J., Saltelli, A., 2007. An effective screening design for sensitivity analysis of large models. Environmental Modelling Software, Modelling, computer-assisted simulations, and mapping of dangerous phenomena for hazard assessment 22, 1509–1518. https://doi.org/10.1016/j.envsoft.2006.10.0

Cárdenas López, J.J., Romero Perdomo, N.M., 2017. Análisis de contaminantes en el agua para consumo humano de la población urbana del municipio de Coello (Tolima, Colombia) (Thesis).

Carrijo, D.R., Lundy, M.E., Linquist, B.A., 2017. Rice yields and water use under alternate wetting and drying irrigation: A meta-analysis. Field Crops Research 203, 173–180.

Casa, A. de la, Ovando, G., Bressanini, L., Martínez, J., 2013. Aquacrop Model Calibration in Potato and Its Use to Estimate Yield Variability under Field Conditions. Atmospheric and Climate Sciences 3, 397–407. https://doi.org/10.4236/acs.2013.33041

Christensen, J.H., Kanikicharla, K.K., Aldrian, E., An, S.I., Cavalcanti, I.F.A., de Castro, M., Dong, W., Goswami, P., Hall, A., Kanyanga, J.K., 2013. Climate phenomena and their relevance for future regional climate change, in: Climate Change 2013 the Physical Science Basis: Working Group I Contribution to the Fifth Assessment Report of the Intergovernmental Panel on Climate Change. Cambridge University Press, pp. 1217–1308.

Coudron, W., Gobin, A., Boeckaert, C., De Cuypere, T., Lootens, P., Pollet, S., Verheyen, K., De Frenne, P., De Swaef, T., 2021. Data collection design for calibration of crop models using practical identifiability analysis. Computers and Electronics in Agriculture 190, 106457.

Coy Tacha, C.A., 2015. Efecto de cuatro épocas de siembra sobre el comportamiento agronómico de cinco variedades comerciales de arroz (oryza sativa) en el centro de investigación Santa Rosa, Villavicencio. Colombia.

Cusicanqui, J., Dillen, K., Garcia, M., Geerts, S., Raes, D., Mathijs, E., 2013. Economic assessment at farm level of the implementation of deficit irrigation for quinoa production in the Southern Bolivian Altiplano. Spanish Journal of Agricultural Research 11, 894–907. https://doi.org/10.5424/sjar/2013114-4097

De Pauw, D.J.W., Steppe, K., De Baets, B., 2008. Identifiability analysis and improvement of a tree water flow and storage model. Mathematical Biosciences 211, 314–332. https://doi.org/10.1016/j.mbs.2007.08.007

Diepen, C.A. van, Voet, P. van der, 1998. Application of simple interpolation methods in agrometeorology.

Dixneuf, P., 2019. Analyse de la performance de la méthode d'imputation de données manquantes missForest et application à des données environnementales (masters No. 2019:2). École de technologie supérieure, Montréal.

Durfee, N., Ochoa, C.G., Mata-Gonzalez, R., 2019. The use of low-altitude UAV imagery to assess western juniper density and canopy cover in treated and untreated stands. Forests 10, 296.

Dutta, M., Prasad, R., Kumar, J., Saini, G.C., 1996. Heading and spikelet fertility in cold tolerant rice genotypes as influenced by environments in high altitude area. Indian Journal of Plant Genetic Resources 9, 73–79.

Ebrahim, A., Hamidreza, A.A., Aimrun, W., Mojtaba, R., 2015. SIMULATION OF RICE YIELD UNDER WATER AND SALINITY STRESS IN RASHT AREA USING AQUACROP MODEL. Jurnal Teknologi 76. https://doi.org/10.11113/jt.v76.5947

Echeverri, J., Beltrán, J., Amezquita, N., 2019. EFECTO DE AÑUBLO BACTERIAL SOBRE EL RENDIMIENTO DE SEIS GENOTIPOS DE ARROZ.

Fageria, N.K., 2007. Yield Physiology of Rice. Journal of Plant Nutrition 30, 843–879. https://doi.org/10.1080/

Fageria, N.K., Baligar, V.C., 1999. Yield and yield components of lowland rice as influenced by timing of nitrogen fertilization. Journal of Plant Nutrition 22, 23–32.

FAO, 2021. The state of the world's land and water resources for food and agriculture: managing systems at risk. Earthscan. Fedearroz, 2022. Fenologia de arroz F67 F68.

Fedearroz, 2017. Arroz 70 años, orguillosos de nuestra historia 65, 57–62.

Federación Nacional de Arroceros - Fondo Nacional del Arroz., 2021. División de Investigaciones Económicas. (2021). Cultivo de arroz en Colombia 1988 – 2016: cambios espaciales.

Fernández, M., 2013. Efectos del cambio climático en el rendimiento de tres cultivos mediante el uso del Modelo AquaCrop. FONADE, BID, IDEAM. Informe final. Contrato de Cooperación CO-

T1150.

Fischer, G., Nachtergaele, F.O., van Velthuizen, H., Chiozza, F., Francheschini, G., Henry, M., Muchoney, D., Tramberend, S., 2021. Global agro-ecological zones (gaez v4)-model documentation.

Fraisse, C.W., Breuer, N.E., Zierden, D., Bellow, J.G., Paz, J., Cabrera, V.E., Garcia y Garcia, A., Ingram, K.T., Hatch, U., Hoogenboom, G., Jones, J.W., O'Brien, J.J., 2006. AgClimate: A climate forecast information system for agricultural risk management in the southeastern USA. Computers and Electronics in Agriculture 53, 13–27. https://doi.org/10.1016/j.compag.2006.03.002

Garofalo, P., Ventrella, D., Kersebaum, K.C., Gobin, A., Trnka, M., Giglio, L., Dubrovský, M., Castellini, M., 2019. Water footprint of winter wheat under climate change: Trends and uncertainties associated to the ensemble of crop models. Science of The Total Environment 658, 1186–1208. https://doi.org/10.1016/j.scitotenv.2018.12.279

Geerts, S., Raes, D., Garcia, M., 2010. Using AquaCrop to derive deficit irrigation schedules. Agricultural Water Management 98, 213–216. https://doi.org/10.1016/j.agwat.2010.07.003

Ghildyal, B., Satyanarayana, T., 1965. Effects of compaction on the physical properties of four different soils in India. Journal of the Indian Society of Soil Science 55.

Gleick, P.H., Palaniappan, M., 2010. Peak water limits to freshwater withdrawal and use. Proceedings of the National Academy of Sciences 107, 11155–11162.

Gnyp, M.L., Yu, K., Aasen, H., Yao, Y., Huang, S., Miao, Y., Bareth, G., 2013. Analysis of Crop Reflectance for Estimating Biomass in Rice Canopies at Different Phenological Stages. Photogrammetrie - Fernerkundung - Geoinformation 351–365. https://doi.org/10.1127/1432-8364/2013/0182

Gobin, A., Kersebaum, K.C., Eitzinger, J., Trnka, M., Hlavinka, P., Takáč, J., Kroes, J., Ventrella, D., Marta, A.D., Deelstra, J., Lalić, B., Nejedlik, P., Orlandini, S., Peltonen-Sainio, P., Rajala, A., Saue, T., Şaylan, L., Stričevic, R., Vučetić, V., Zoumides, C., 2017. Variability in the Water Footprint of Arable Crop Production across European Regions. Water 9, 93. https://doi.org/10.3390/w9020093

Gogoi, N.K., Deka, B., Bora, L.C., 2018. Remote sensing and its use in detection and monitoring plant diseases: A review. Agricultural Reviews 39.

Gomezcasseres Argumedo, L.M., 2021. Análisis agronómico de seis variedades de arroz (Oryza sativa) en función de diferentes épocas de siembra en el Centro Experimental La Victoria Fedearroz-Montería.

González B, M., Alonso, A.M., 2016. Tecnologías para ahorrar agua en el cultivo de arroz. NOVA publ. cient 63–78.

Gonzalez, M.C., Saldarriaga, G., Jaramillo, O., 2010. Estimación de la demanda de agua. IDEAM, Estudio Nacional del Agua. Granados Thorin, N., 2021. Evaluación de efectividad de bacterias promotoras de crecimiento vegetal en la variedad de arroz F67 (Oryza sativa).

Greenland, D.J., Pereira, H.C., Cooke, G.W., Pirie, N.W., Bell, G.D.H., 1977. Soil damage by intensive arable cultivation: temporary or permanent? Philosophical Transactions of the Royal Society of London. B, Biological Sciences 281, 193–208. https://doi.org/10.1098/rstb.1977.0133

He, D., Wang, E., Wang, J., Robertson, M.J., 2017. Data requirement for effective calibration of process-based crop models. Agricultural and Forest Meteorology 234–235, 136–148. https://doi.org/10.1016/j.agrfo

Henry, A., Gowda, V.R.P., Torres, R.O., McNally, K.L., Serraj, R., 2011. Variation in root system architecture and drought response in rice (Oryza sativa): Phenotyping of the OryzaSNP panel in rainfed lowland fields. Field Crops Research 120, 205–214. https://doi.org/10.1016/j.fcr.2010.10.003

Heros, E., Díaz, J., Donoso, G., Becerra, V., 2022. MÁS ARROZ CON MENOS EMISIONES Y MENOR CONSUMO DE AGUA.

Herrera Vidal, A.F., 2020. Manejo agronómico de variedades de arroz (oryza sativa) bajo diferentes épocas de siembra del Centro de Investigación la Victoria Fedearroz - Montería.

Hour sunset and sunrise calculator [WWW Document], n.d. URL https://www.sunrise-and-sunset.com/fr/sun/c (accessed 7.16.22).

Hsiao, T.C., Heng, L., Steduto, P., Rojas-Lara, B., Raes, D., Fereres, E., 2009. AquaCrop—The FAO Crop Model to Simulate Yield Response to Water: III. Parameterization and Testing for Maize. Agronomy Journal 101, 448–459. https://doi.org/10.2134/agronj2008.0218s

IDEAM, U., 2018. La variabilidad climática y el cambio climático en Colombia. Bogotá: IDEAM. Available online at: http://www. andi. com. co/Uploads/variabilidad. pdf.

IGAC, 2004. Estudio general de suelos y zonificación de tierras. Departamento del Tolima. Escala 1: 100000.

IRI, n.d. IRI Data Library What's New • UCSB CHIRPS Version 2.0 Precipitation Analyses... [WWW Document]. IRI Data Library What's New. URL https://iridl.tumblr.com/post/111396662121/ucsb-chirps-version-2-0-precipitation-analyses (accessed 8.5.22). IRRI, 1994. International Rice Research Notes. Int. Rice Res. Inst.

Jägermeyr, J., Gerten, D., Heinke, J., Schaphoff, S., Kummu, M., Lucht, W., 2015. Water savings potentials of irrigation systems: Global simulation of processes and linkages. Hydrology and Earth System Sciences 19, 3073–3091. https://doi.org/10.5194/hess-19-3073-2015

Jennings, P.R., 1979. Rice Improvement. Int. Rice Res. Inst.

Jiménez-Jiménez, S.I., Ojeda-Bustamante, W., InzunzaIbarra, M.A., Marcial-Pablo, M.J., 2021. Analysis of the NASA-POWER system for estimating reference evapotranspiration in the Comarca Lagunera, Mexico. Ingeniería Agrícola y Biosistemas 13, 201–226.

Jones, J.W., Hoogenboom, G., Porter, C.H., Boote, K.J., Batchelor, W.D., Hunt, L.A., Wilkens, P.W., Singh, U., Gijsman, A.J., Ritchie, J.T., 2003. The DSSAT cropping system model. European Journal of Agronomy, Modelling Cropping Systems: Science, Software and Applications 18, 235–265. https://doi.org/10.1016/S1161-0301(02)00107-7

Kersebaum, K.C., Kroes, J., Gobin, A., Takáč, J., Hlavinka, P., Trnka, M., Ventrella, D., Giglio, L., Ferrise, R., Moriondo, M., Dalla Marta, A., Luo, Q., Eitzinger, J., Mirschel, W., Weigel, H.-J., Manderscheid, R., Hoffmann, M., Nejedlik, P., Iqbal, M.A., Hösch, J., 2016. Assessing Uncertainties

of Water Footprints Using an Ensemble of Crop Growth Models on Winter Wheat. Water 8, 571. https://doi.org/10.3390/w8120571

Kirby, J.M., Kirchhof, G., 1990. The compaction process and factors affecting soil compactibility. Kozaka, T., 1961. Ecological studies on sheath blight of rice plant caused by Pellicularia sasakii and its chemical control. Chugoku Agric. Res 20, 1–13.

Kropff, M.J., Van Laar, H.H., Matthews, R.B., 1994. ORYZA1: An ecophysiological model for irrigated rice production. Lal, R., 2021. Chapter 31 - Climate change and agriculture, in: Letcher, T.M. (Ed.), Climate Change (Third Edition). Elsevier, pp. 661–686. https://doi.org/10.1016/B978-0-12-821575-3.00031-1

Lampayan, R.M., Samoy-Pascual, K.C., Sibayan, E.B., Ella, V.B., Jayag, O.P., Cabangon, R.J., Bouman, B.A.M., 2015. Effects of alternate wetting and drying (AWD) threshold level and plant seedling age on crop performance, water input, and water productivity of transplanted rice in Central Luzon, Philippines. Paddy and Water Environment 13, 215–227.

Liu, X., Xiao, X., Yang, G., Ren, T., 2011. Water Retention Curves of Soil Aggregates as Affected by Long-Term Fertilizer Management. Soil Science 176, 537–542. https://doi.org/10.1097/SS.0b013e31822af68d

Lozano, L.A.C., Ospina, Y.C.T., 2019. FUNDAMENTOS TÉCNICOS PARA LA NUTRICIÓN DEL CULTIVO DE ARROZ. Lu, S., Yu, X., Zong, Y., 2019. Nano-microscale porosity and pore size distribution in aggregates of paddy soil as affected by long-term mineral and organic fertilization under rice-wheat cropping system. Soil and Tillage Research 186, 191–199. https://doi.org/10.1016/j.still.2018.10.008

Luna Carlosama, C.F., Moreno Chuquen, R., Mulcue Nieto, L.F., Jiménez García, F.N., 2021. Potential of Photovoltaic Generation in the Putumayo Department of Colombia. Applied Sciences 11, 5528.

Marshall, T.J., Holmes, J.W., Rose, C.W., 1996. Soil Physics. Cambridge University Press.

Maurya, A.K., Singh, D., Singh, K.P., 2018. Development of fusion approach for estimation of vegetation fraction cover with drone and sentinel-2 data, in: IGARSS 2018-2018 IEEE International Geoscience and Remote Sensing Symposium. IEEE, pp. 7448–7451.

Melo Solarte, M.A., 2019. Calibración de modelo agrometereológico Aquacrop para evaluar el rendimiento del arroz bajo riego inundado con alternancia de humedecimiento y secado. Universidad Nacional Agraria La Molina.

Mirfenderski, R., Darzi-Naftchali, A., Karandish, F., 2022. Climate-resilient agricultural water management to alleviate negative impacts of global warming in rice production systems. Theor Appl Climatol 147, 409–422. https://doi.org/10.1007/s00704-021-03813-8

Miro, B., Ismail, A., 2013. Tolerance of anaerobic conditions caused by flooding during germination and early growth in rice (Oryza sativa L.). Frontiers in Plant Science 4.

Moriasi, D.N., Arnold, J.G., Van Liew, M.W., Bingner, R.L., Harmel, R.D., Veith, T.L., 2007. Model evaluation guidelines for systematic quantification of accuracy in watershed simulations. Transactions of the ASABE 50, 885–900.

Morris, M.D., 1991. Factorial sampling plans for preliminary computational experiments. Technometrics 33, 161–174.

Mote, K., Rao, V.P., Ramulu, V., Kumar, K.A., Devi, M.U., 2022. Performance of rice (Oryza sativa (L.)) under AWD irrigation practice—A brief review. Paddy Water Environ 20, 1–21. https://doi.org/10.1007/s10333-021-00873-4

Muff, S., Nilsen, E.B., O'Hara, R.B., Nater, C.R., 2022. Rewriting results sections in the language of evidence. Trends in Ecology Evolution 37, 203–210. https://doi.org/10.1016/j.tree.2021.10.009

Myneni, R.B., Hall, F.G., Sellers, P.J., Marshak, A.L., 1995. The interpretation of spectral vegetation indexes. IEEE Trans. Geosci. Remote Sensing 33, 481–486. https://doi.org/10.1109/36.377948

NASA, 2020. NASA POWER | Docs | Methodology - NASA POWER | Docs [WWW Document]. URL https://power.larc.nasa.gov/docs/methodology/ (accessed 8.5.22).

Ndiaye, P.M., Bodian, A., Diop, L., Deme, A., Dezetter, A., Djaman, K., Ogilvie, A., 2020. Trend and sensitivity analysis of reference evapotranspiration in the Senegal river basin using NASA meteorological data. Water 12, 1957.

Nelson, D. a, Sommers, L., 1983. Total carbon, organic carbon, and organic matter. Methods of soil analysis: Part 2 chemical and microbiological properties 9, 539–579.

Neupane, J., Guo, W., 2019. Agronomic Basis and Strategies for Precision Water Management: A Review. Agronomy 9, 87. https://doi.org/10.3390/agronomy9020087

Niu, Y., Han, W., Zhang, H., Zhang, L., Chen, H., 2021. Estimating fractional vegetation cover of maize under water stress from UAV multispectral imagery using machine learning algorithms. Computers and Electronics in Agriculture 189, 106414. https://doi.org/10.1016/j.compag.2021.106414

Norton, G.J., Shafaei, M., Travis, A.J., Deacon, C.M., Danku, J., Pond, D., Cochrane, N., Lockhart, K., Salt, D., Zhang, H., 2017. Impact of alternate wetting and drying on rice physiology, grain production, and grain quality. Field Crops Research 205, 1–13. Ocampo Henao, L.F., 2019. Informe final pasantía Hacienda San Javier.

Omlin, M., Brun, R., Reichert, P., 2001. Biogeochemical model of Lake Zürich: sensitivity, identifiability and uncertainty analysis. Ecological Modelling 141, 105–123. https://doi.org/10.1016/S0304-3800(01)00257-5

O'toole, J.C., 1982. Adaptation of rice environments. Drought Resistance in Crops with Emphasis on Rice; Paddyfield: Manila, Philippines 195–213.

O'Toole, J.C., Bland, W.L., 1987. Genotypic Variation in Crop Plant Root Systems, in: Brady, N.C. (Ed.), Advances in Agronomy. Academic Press, pp. 91–145. https://doi.org/10.1016/S0065-2113(08)60803-2

Peniad Suarez, D.F., 2020. Manejo eficiente del agua para la produccion sostenible de arroz en Colombia.

Pereira, L.S., Perrier, A., Allen, R.G., Alves, I., 1996. Evapotranspiration: Review of concepts and

future trends, in: International Conference. ASAE.

Philip, J.R., 1957. The theory of infiltration: 1. The infiltration equation and its solution. Soil science 83, 345–358.

Porras-Jorge, R., Ramos-Fernández, L., Ojeda-Bustamante, W., Ontiveros-Capurata, R.E., 2020. Performance assessment of the AquaCrop model to estimate rice yields under alternate wetting and drying irrigation in the coast of Peru. Scientia Agropecuaria 11, 309–321.

Prescott, A., 1940. Evaporation from a water surface in relation to solar radiation. Trans. Roy. Soc. S. Aust. 46, 114–118. Price, A.H., Norton, G.J., Salt, D.E., Ebenhoeh, O., Meharg, A.A., Meharg, C., Islam, M.R., Sarma, R.N., Dasgupta, T., Ismail, A.M., 2013. Alternate wetting and drying irrigation for rice in Bangladesh: Is it sustainable and has plant breeding something to offer? Food and Energy Security 2, 120–129.

Price, A.H., Tomos, A.D., Virk, D.S., 1997. Genetic dissection of root growth in rice (Oryza sativa L.)I: a hydrophonic screen. Theor Appl Genet 95, 132–142. https://doi.org/10.1007/s001220050541

Raes, D., Steduto, P., Hsiao, T.C., Fereres, E., 2018a. Chapter 1: FAO crop-water productivity model to simulate yield response to water: AquaCrop: version 6.0-6.1: reference manual. Rome: FAO, 2018b. 19p.

Raes, D., Steduto, P., Hsiao, T.C., Fereres, E., 2018b. Chapter 2: Users guide. AquaCrop version 6.0-6.1. Reference Manual. Food Agricultural Organization (FAO), Rome 2–302.

Raes, D., Steduto, P., Hsiao, T.C., Fereres, E., 2009. AquaCrop—The FAO Crop Model to Simulate Yield Response to Water: II. Main Algorithms and Software Description. Agronomy Journal 101, 438–447. https://doi.org/10.2134/agronj2008.0140s

Redagricola, 2021. Producción y mercado del arroz en Colombia [WWW Document]. Redagrícola Colombia. URL https://www.redagricola.com/co/produccion-y-mercado-del-arroz-en-colombia/ (accessed 7.29.22).

Reed, B.C., Brown, J.F., VanderZee, D., Loveland, T.R., Merchant, J.W., Ohlen, D.O., 1994. Measuring phenological variability from satellite imagery. Journal of Vegetation Science 5, 703–714. https://doi.org/10.2307/3235884

Resop, J.P., Fleisher, D.H., Wang, Q., Timlin, D.J., Reddy, V.R., 2012. Combining explanatory crop models with geospatial data for regional analyses of crop yield using field-scale modeling units. Computers and Electronics in Agriculture 89, 51–61. https://doi.org/10.1016/j.compag.2012.08.001

RIceClimaRemote, 2021. First annual technical report “RiceClimaRemote.”

Richey, A.S., Thomas, B.F., Lo, M.-H., Reager, J.T., Famiglietti, J.S., Voss, K., Swenson, S., Rodell, M., 2015. Quantifying renewable groundwater stress with GRACE. Water Resources Research 51, 5217–5238. https://doi.org/10.1002/2015WR017349

Rosenzweig, C., Elliott, J., Deryng, D., Ruane, A.C., Müller, C., Arneth, A., Boote, K.J., Folberth, C., Glotter, M., Khabarov, N., Neumann, K., Piontek, F., Pugh, T.A.M., Schmid, E., Stehfest, E., Yang, H., Jones, J.W., 2014. Assessing agricultural risks of climate change in the 21st century in a

global gridded crop model intercomparison. Proceedings of the National Academy of Sciences 111, 3268–3273. https://doi.org/10.1073/pnas.1222463110

Saadati, Z., Pirmoradian, N., Rezaei, M., 2011. CALIBRATION AND EVALUATION OF AQUACROP MODEL IN RICE GROWTH SIMULATION UNDER DIFFERENT IRRIGATION MANAGEMENTS.

Saltelli, A., Tarantola, S., Chan, K.P.-S., 1999. A Quantitative Model-Independent Method for Global Sensitivity Analysis of Model Output. Technometrics 41, 39–56. https://doi.org/10.1080/00401706.1999.104

Sarmad, M., 2006. Robust data analysis for factorial experimental designs: Improved methods and software (PhD Thesis). Durham University.

SATREPS, 2019. Desarrollo y Adopción de un Sistema de Producción de Arroz de Bajo Uso de Insumos para Latinoamérica a través de Mejoramiento Genético y Tecnologías Avanzadas de Manejo del Cultivo.

Sauer, T., Havlík, P., Schneider, U.A., Schmid, E., Kindermann, G., Obersteiner, M., 2010. Agriculture and resource availability in a changing world: The role of irrigation. Water Resources Research 46. https://doi.org/10.1029/2009WR007729

Saxton, K.E., Rawls, W., Romberger, J.S., Papendick, R.I., 1986. Estimating generalized soil-water characteristics from texture. Soil science society of America Journal 50, 1031–1036.

Schaap, M.G., Leij, F.J., Van Genuchten, M.T., 2001. Rosetta: A computer program for estimating soil hydraulic parameters with hierarchical pedotransfer functions. Journal of hydrology 251, 163–176.

Schmitter, P., Dercon, G., Hilger, T., Ha, T., Thanh, N., Lam, N., Vien, T., Cadisch, G., 2010. Sediment induced soil spatial variation in paddy fields of Northwest Vietnam. Geoderma 155, 298–307. https://doi.org/10.1016/j.geoderma.2009.12.014 Service (NRCS), N.R.C., 2004. National engineering handbook.

Shah, T., 1985. Transforming groundwater markets into powerful instrument of small farmer development. ODI Irrigation Management Network Paper.

Sheehy, J.E., Mitchell, P.L., 2013. Designing rice for the 21st century: the three laws of maximum yield. Discuss Paper Series 48, 19.

Shwetha, P., Varija, K., 2015. Soil water retention curve from saturated hydraulic conductivity for sandy loam and loamy sand textured soils. Aquatic Procedia 4, 1142–1149.

Siebert, S., Kummu, M., Porkka, M., Döll, P., Ramankutty, N., Scanlon, B.R., 2015. A global data set of the extent of irrigated land from 1900 to 2005. Hydrology and Earth System Sciences 19, 1521–1545. https://doi.org/10.5194/hess-19-1521-2015

Sin, G., Gernaey, K.V., 2009. Improving the Morris method for sensitivity analysis by scaling the elementary effects, in: Computer Aided Chemical Engineering. Elsevier, pp. 925–930.

Singh, A., Saha, S., Mondal, S., 2013. MODELLING IRRIGATED WHEAT PRODUCTION USING THE FAO AQUACROP MODEL IN WEST BENGAL, INDIA, FOR SUSTAINABLE AGRICULTURE. Irrigation and Drainage 62, 50–56.

Steduto, P., Hsiao, T.C., Fereres, E., Raes, D., 2012. Crop yield response to water. Food and Agriculture Organization of the United Nations Rome.

Steduto, P., Hsiao, T.C., Raes, D., Fereres, E., 2009. AquaCrop—The FAO Crop Model to Simulate Yield Response to Water: I. Concepts and Underlying Principles. Agronomy Journal 101, 426–437. https://doi.org/10.2134/agronj2008.0139s

Stekhoven, D.J., Bühlmann, P., 2012. MissForest—non-parametric missing value imputation for mixed-type data. Bioinformatics 28, 112–118.

Stöckle, C.O., Donatelli, M., Nelson, R., 2003. CropSyst, a cropping systems simulation model. European Journal of Agronomy, Modelling Cropping Systems: Science, Software and Applications 18, 289–307. https://doi.org/10.1016/S1161-0301(02)00109-0 Tacker, P., Vories, E., Kratz, D., 2007. Rice irrigation-water management for water, labor, and cost savings. RICE RESEARCH STUDIES 2002 338.

Tirado, Y., Castilla Lozano, L.A., 2017. EXITOSO RESULTADO DEL PROYECTO DE MANEJO AGRONÓMICO POR AMBIENTE. REVISTA ARROZ 65, 38–45. Tirol-Padre, A., Ladha, J.K., Singh, U., Laureles, E., Punzalan, G., Akita, S., 1996. Grain yield performance of rice genotypes at suboptimal levels of soil N as affected by N uptake and utilization efficiency. Field Crops Research 46, 127–143. https://doi.org/10.1016/0378-4290(95)00095-X

Todorovic, M., Albrizio, R., Zivotic, L., Saab, M.-T.A., Stöckle, C., Steduto, P., 2009. Assessment of AquaCrop, CropSyst, and WOFOST Models in the Simulation of Sunflower Growth under Different Water Regimes. Agronomy Journal 101, 509–521. https://doi.org/10.2134/agronj2008.0166s

Touré, A., Major, D.J., Lindwall, C.W., 1995. Comparison of five wheat simulation models In southern Alberta. Can. J. Plant Sci. 75, 61–68. https://doi.org/10.4141/cjps95-010

United Nations, 2017. World Population Prospects: The 2017 Revision, Key Findings and Advance Tables. Department of Economic and Social Affairs, Population Division: New York, NY, USA 248.

United States Departement of Agriculture, 2014. Keys to Soil Taxonomy. Government Printing Office.

van Buuren, S., 2022. https://stefvanbuuren.name/fimd/sec-MCAR.html.

Vanuytrecht, E., Raes, D., Steduto, P., Hsiao, T.C., Fereres, E., Heng, L.K., Garcia Vila, M., Mejias Moreno, P., 2014a. AquaCrop: FAO's crop water productivity and yield response model. Environmental Modelling Software 62, 351–360. https://doi.org/10.1016/j.envsoft.2014.08.005

Vanuytrecht, E., Raes, D., Willems, P., 2014b. Global sensitivity analysis of yield output from the water productivity model. Environmental Modelling Software 51, 323–332. https://doi.org/10.1016/j.envsoft.2013.

Wang, L., Zhang, F., Jing, Y., Jiang, X., Yang, S., Han, X., 2014. Multi-Temporal Detection of Rice Phenological Stages Using Canopy Spectrum. Rice Science 21, 108–115. https://doi.org/10.1016/S1672-6308(13)60170-5

Wayayok, A., Amin, M., 2009. Pedo-transfer function for saturated hydraulic conductivity of

lowland paddy soils. Paddy and Water Environment 7, 217–225. https://doi.org/10.1007/s10333-009-0165-y

Wopereis, M.C.S., Kropff, M.J., Maligaya, A.R., Tuong, T.P., 1996. Drought-stress responses of two lowland rice cultivars to soil water status. Field Crops Research 46, 21–39.

Wösten, J.H.M., Lilly, A., Nemes, A., Le Bas, C., 1999. Development and use of a database of hydraulic properties of European soils. Geoderma 90, 169–185.

Zeleke, K.T., 2019. AquaCrop Calibration and Validation for Faba Bean (Vicia faba L.) under Different Agronomic Managements. Agronomy 9, 320. https://doi.org/10.3390/agronomy9060320

Zhai, B., Fu, Q., Li, T., Liu, D., Ji, Y., Li, M., Cui, S., 2019. Rice Irrigation Schedule Optimization Based on the AquaCrop Model: Study of the Longtouqiao Irrigation District. Water 11, 1799. https://doi.org/10.3390/w11091799

Zhang, D., Zhou, X., Zhang, J., Huang, L., Zhao, J., 2017. Developing a small UAV platform to detect sheath blight of rice, in: 2017 IEEE International Geoscience and Remote Sensing Symposium (IGARSS). pp. 3190–3193. https://doi.org/10.1109/IGARSS.2017.8127675

N.d. URL https://cursosgis.com/ (accessed 7.16.22).